frontiers in Earth Science

ORIGINAL RESEARCH
published: 07 June 2021
doi: 10.3389/feart.2021.670952

Combined On-Fault and Off-Fault Paleoseismic Evidence in the Postglacial Infill of the Inner-Alpine Lake Achensee (Austria, Eastern Alps)

Patrick Oswald[1], Jasper Moernaut[1], Stefano C. Fabbri[2], Marc De Batist[3], Irka Hajdas[4], Hugo Ortner[1], Sebastian Titzler[1] and Michael Strasser[1]*

[1]Department of Geology, University of Innsbruck, Innsbruck, Austria, [2]Institute of Geological Sciences and Oeschger Centre for Climate Change Research, University of Bern, Bern, Switzerland, [3]Department of Geology, Ghent University, Ghent, Belgium, [4]Laboratory of Ion Beam Physics, ETH Zürich, Zürich, Switzerland

The Eastern European Alps are characterized by slow active deformation with low- to moderate seismicity. Recurrence rates of severe earthquakes exceed the time span of historical documentation. Therefore, historical and instrumental earthquake records might be insufficient for seismic hazard assessment and high-quality paleoseismic data is required. However, primary geological observations of postglacial fault activity are scarcely found, because major faults are buried below thick sedimentary sequences in glacially overdeepened valleys. Moreover, high erosion rates, gravitational slope processes and penetrative anthropogenic landscape modification often obscure geomorphic features related to surface ruptures. Here we present one of the rare paleoseismic data sets showing both on-fault evidence as subaqueous surface ruptures and off-fault evidence as multiple coeval mass-transport deposits (MTDs) and megaturbidites within a single high-resolution seismic-stratigraphic framework of the inner-alpine lake Achensee. Co-occurrence of on-fault and off-fault paleoseismic evidence on three stratigraphic levels indicates seismic activity with inferred moment magnitudes M_W ~6–6.5 of the local, lake-crossing Sulzgraben-Eben thrust at ~8.3 ka BP and twice in Late Glacial times. Additional eight stratigraphic levels with only off-fault paleoseismic evidence document severe seismic shaking related to the historical M_W ~5.7 earthquake in Hall (CE 1670) and seven Holocene earthquakes, which have exceeded a local seismic intensity of ~VI (EMS-98) at Achensee. Furthermore, we discuss natural and methodological influencing factors and potential pitfalls for the elaboration of a subaqueous paleoseismic record based on surface ruptures and multiple, coeval MTDs.

Keywords: lacustrine paleoseismology, active tectonics, earthquake, surface rupture, mass-transport deposit, Eastern Alps

OPEN ACCESS

Edited by:
Hector Perea, Complutense University of Madrid, Spain

Reviewed by:
Kiichiro Kawamura, Yamaguchi University, Japan
Gueorgui Ratzov, Université Côte d'Azur, France

****Correspondence:***
Patrick Oswald
Patrick.Oswald@uibk.ac.at

Specialty section:
This article was submitted to Structural Geology and Tectonics, a section of the journal Frontiers in Earth Science

Received: *22 February 2021*
Accepted: *17 May 2021*
Published: *07 June 2021*

Citation:
Oswald P, Moernaut J, Fabbri SC, De Batist M, Hajdas I, Ortner H, Titzler S and Strasser M (2021) Combined On-Fault and Off-Fault Paleoseismic Evidence in the Postglacial Infill of the Inner-Alpine Lake Achensee (Austria, Eastern Alps). Front. Earth Sci. 9:670952. doi: 10.3389/feart.2021.670952

INTRODUCTION

The European Alps are a slowly but actively deforming orogen with an overall convergence rate of 1–2 mm/year between the counter-clockwise rotating Adriatic plate and a stable European plate (Métois et al., 2015). Moreover, excessive uplift rates—beyond what is expected from postglacial isostatic rebound—indicate neotectonic activity especially in the Eastern Alps (Mey et al., 2016).

Present-day seismicity in the Eastern Alps is moderate, at shallow depths (5–10 km) and concentrated in specific regions e.g. in central Tyrol (Reiter et al., 2018; **Figure 1A**), where also severe and damaging earthquakes are historically documented (e.g., Hall M_W ~5.7 in CE 1670; Stucchi et al., 2013). For these severe historical earthquakes, the epicentral location or the magnitude is often debated and therefore, also the causative faults remain unknown. Moreover, severe earthquakes for a given region in the Alps tend to have long recurrence intervals in the order of 1,000–2,000 years (e.g., Kremer et al., 2020) with complex and clustered recurrence patterns (Oswald et al., 2021). Therefore, historical and instrumental earthquake records might be insufficient for seismic hazard assessment. For several parts of the Alps, advanced understanding of severe earthquake recurrence has been gained from long Holocene paleo-earthquake records established in lake sediments (e.g., Beck et al., 1996; Kremer et al., 2017; Rapuc et al., 2018). Lacustrine paleoseismology takes advantage of the often high-resolution, continuous and accurately datable sedimentary succession in lakes, while being sensitive for seismic shaking and able to preserve sedimentary imprints of earthquakes (Strasser et al., 2013). Such off-fault paleoseismic evidence, when documented at multiple lake sites and interpreted to be coeval, can be used to evaluate epicentral locations and magnitudes of paleo-earthquakes by constraining intensity threshold conditions at each lake site and applying empirical seismic attenuation relation in a grid-search approach (Strasser et al., 2006; Kremer et al., 2017). Yet, the causative source fault for the majority of severe earthquakes in the Alps remains not constrained.

Major tectonic faults occur along the main longitudinal valleys in the Eastern Alps (Robl and Stüwe, 2005) indicating that the faults partially controlled the pathway of glacial and fluvial erosion and thus also valley formation. Nowadays, these major faults are mostly buried below glacially overdeepened valleys filled with hundreds of meters thick peri- to postglacial sediments (Preusser et al., 2010), which makes geological observations of possible neotectonic activity by e.g., fault trenching not applicable. Moreover, the faults in the basement rocks and their possible postglacial surface ruptures within such thick sedimentary successions can often not be resolved even with high-resolution land-seismic reflection imaging (Burschil et al., 2019). In Alpine areas with less postglacial sediment cover, the preservation of on-fault paleoseismic evidence is potentially limited by i) penetrative anthropogenic landscape modification in often densely populated valleys, ii) gravitational slope processes or iii) relatively high erosion rates in a moderate-humid Alpine climate (Ustaszewski and Pfiffner, 2008). Especially normal faults can be well preserved in steep terrain, however, the scarceness of glacial and post-glacial sediments overlying these faults prohibits the stratigraphic recording and dating of potential surface ruptures. Only a few specific sites with on-fault evidence of postglacial surface ruptures have been documented within the Alps which were not affected by abovementioned limitations. Displaced Roman archeological remains were linked to seismotectonic deformation at the Egna fault in the Adige Valley, northern Italy (Galadini and Galli, 1999). Tectonically damaged speleothems found in a cave in the Hochschwab massif, eastern Austria, which indicate ongoing lateral extrusion tectonics of the Eastern Alps (Plan et al., 2010). Remote lineament mapping on aerial photographs and subsequent field investigations identified 1,700 tectonic faults in the central and western Swiss Alps, of which only two unequivocally exhibit post-glacial activity (Ustaszewski and Pfiffner, 2008).

Alpine lakes can form another potential geological archive for on-fault paleoseismic evidence as lake basins are often located in fault-aligned valleys or are crossed by major fault systems. So far, faulting in postglacial sediments is only documented by reflection seismic imaging in three Alpine lakes. At Lake Garda in northern Italy, folded strata in the sedimentary infill parallel to onshore fold-related faults and enhanced mass wasting close to interpreted active tectonic features were related to postglacial seismicity (Gasperini et al., 2020). Riedel-type faults offset the sedimentary infill and lake-floor morphology of Lake Le Bourget, northwestern French Alps and were assigned to postglacial-Holocene activity of two onshore-documented strike slip faults (de La Taille et al., 2015). At Lake Thun in central Switzerland, fault traces were identified by amphibious geomorphic and subsurface investigations and attributed to Holocene seismotectonic activity (Fabbri et al., 2017). Even though these studies show evidence for postglacial seismotectonic activity and the great potential use of Alpine lake sequences for on-fault paleoseismology, no quantified paleoseismic data was obtained, such as the number and timing of surface rupturing events or the amount and extent of co-seismic displacement. This is because i) surface ruptures were only visualized in geophysical data without sampling and dating through sediment cores, and ii) surface ruptures could not be tied to specific stratigraphic levels due to missing marker horizons in the stratigraphy or rather low-frequency (and thus low resolution) seismic sources used during the reflection seismic surveys.

In this study, we investigate on-fault as well as off-fault paleoseismic evidence in a single Alpine lake basin (Achensee) in the Eastern Alps by using a dense grid of reflection seismic profiling with two different sources. Furthermore, we evaluate and date potential earthquake-related seismic-stratigraphic event horizons in sediment cores. Semi-quantitative considerations are applied to both on-fault and off-fault paleoseismic evidence and are compared with each other. We discuss i) the natural and methodological factors influencing subaqueous realms in recording remote earthquakes and in preserving subaqueous surface ruptures, ii) implement our paleoseismic results within the regional seismotectonic framework and iii) propose potential source faults of postglacial seismic activity.

SETTING

Seismotectonic Setting

The study area is located in the southern part of the thin-skinned cover nappe stack of the Northern Calcareous Alps within the Cretaceous-Paleogene collisional orogenic belt of the Eastern Alps (**Figures 1A,B**). In the Cenozoic tectonic evolution of the Eastern Alps, NNW-ward pushing of the rigid Adriatic indenter

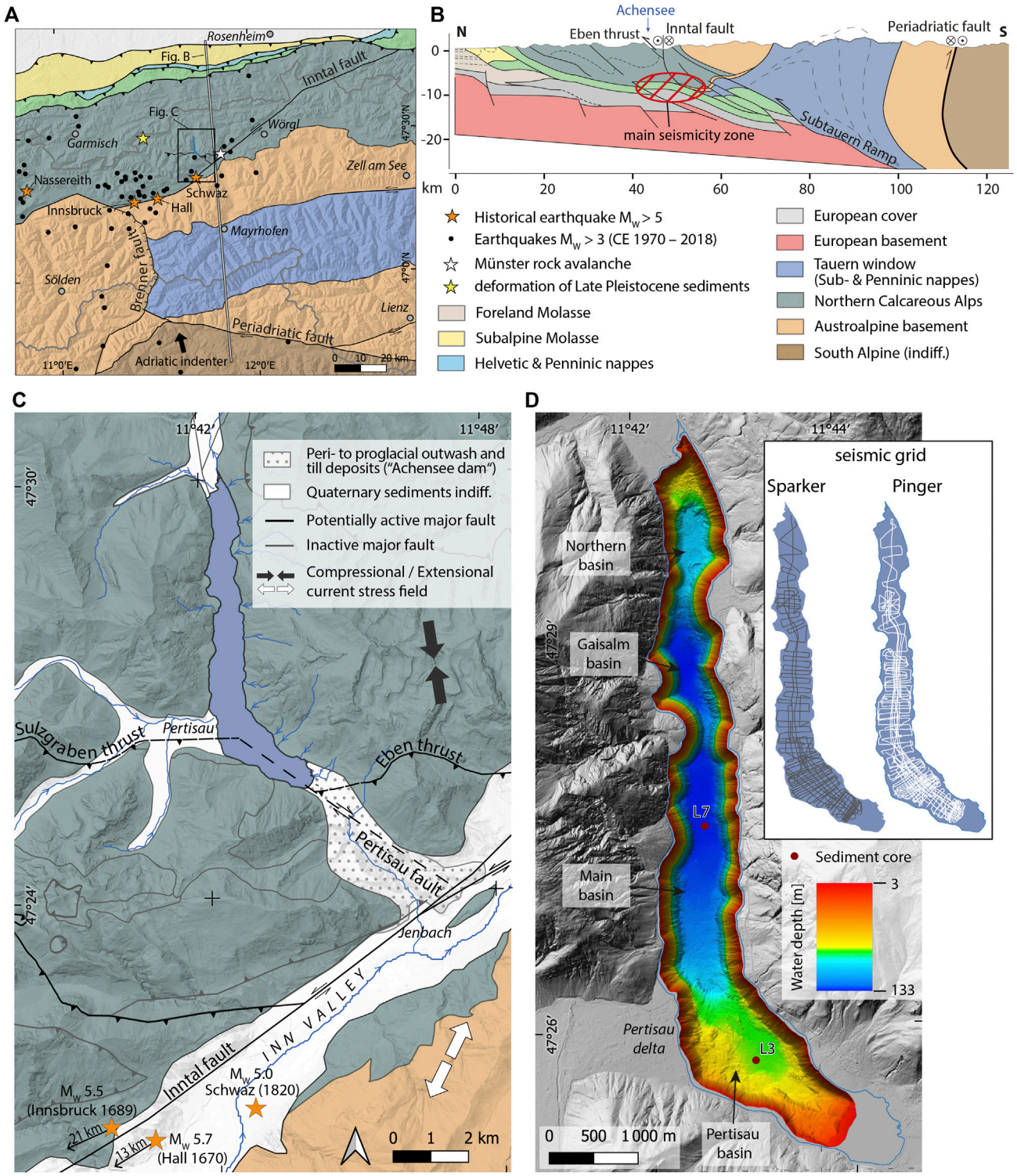

FIGURE 1 | Overview of the study area. **(A)** Seismotectonic map of the central Eastern Alps including the main faults and faults relevant for this study, historical (Stucchi et al., 2013) and recent earthquakes (Reiter et al., 2018), the Münster rock avalanche and deformation in Late Pleistocene sediments of hypothesized neotectonic origin (Costantini and Ortner, 2013). Map modified after Brandner (1980); Bousquet et al. (2012); Geologische Bundesanstalt (2021a, 2021b). **(B)** Simplified cross section across the Eastern Alps indicating the location and depth of the main zone of current seismicity after Reiter et al. (2018) in respect to the major fault systems. Cross section modified after Ortner et al. (2006); Ortner et al. (2015); Reiter et al. (2018). **(C)** Geological map of the surroundings of Achensee. The lake is located within the Northern Calcareous Alps and dammed in the Southeast by proglacial outwash and till deposits accumulated before the Last Glacial Maximum. The

(*Continued*)

FIGURE 1 | southern part of the lake is crosscut by the dextral strike-slip Pertisau fault separating the Sulzgraben and Eben thrusts. The sinistral Inntal fault obliquely crosscuts the Northern Calcareous Alps and separates them from the Austroalpine basement Southeast of Schwaz. The current stress field in this tectonic domain is generally compressional in NNW-SSE direction, but also a NE-SW extensional stress field occurs in the southern part of the study area (Reiter et al., 2018). The historical earthquakes of Hall (CE 1670) and Innsbruck (CE 1689) are located 13 and 21 km to the SW of the map. Earthquake data are derived from Stucchi et al. (2013). Geology and faults modified after Eisbacher and Brandner (1996), Moser (2008), Gruber and Brandner (2012), and Kilian and Ortner (2019). **(D)** Bathymetry of Achensee showing the four sub-basins and the coring sites of this study. Inset shows the dense seismic grid using the pinger (grey) and sparker (white) seismic sources. Onshore digital elevation model is derived from Land Tirol–data.tirol.gv.at.

played a major role (Ratschbacher et al., 1991; Rosenberg et al., 2004; Reiter et al., 2018). In detail, the Alpine front became inactive during the Miocene and shortening migrated more into the hinterland (Ortner et al., 2015), where coeval activity along strike-slip fault systems (e.g., Inntal fault, Periadriatic fault) and normal faults (e.g., Brenner fault) lead to the doming of the Tauern window and E-ward lateral tectonic escape of the Eastern Alps (**Figures 1A,B**; e.g., Ratschbacher et al., 1991; Wölfler et al., 2011).

Nowadays, the Eastern Alps are in a slowly deforming (1–2 mm/year; Métois et al., 2015) intraplate tectonic regime. Apart from that, the Inn valley (southern part of the study area) depicts one of the regions with the highest seismicity in Austria (**Figures 1A,C**; Lenhardt et al., 2007) due to ongoing NNW-ward indentation of the Adriatic microplate (Reiter et al., 2018, and references therein) accumulating stress on existing major faults (e.g., Inntal fault) that are connected with the deep-reaching, S-dipping sub-Tauern ramp (**Figure 1B**; Ortner et al., 2006). Focal mechanism data of recent seismic activity indicate a general NNW-SSE oriented current stress field with predominantly top-North thrusting motions, but also a subordinate NE-SW orogen-parallel and -oblique extension especially in the southern part of the study area (**Figure 1C**; Reiter et al., 2018). Earthquakes are concentrated in a seismic zone at 5–10 km depth below the Inn valley (**Figure 1B**), which attests thrust activity on several major and partly blind, S-dipping faults below and North of the Inn valley. Among these are the Sulzgraben and Eben thrusts, both forming parts of a 21 km long out-of-sequence thrust delimiting one of the major thrust sheets of the Northern Calcareous Alps, hereafter named Sulzgraben-Eben thrust (**Figure 1C**; Kilian and Ortner, 2019). The Sulzgraben-Eben thrust is dissected by the NW-striking, valley-aligned strike-slip Pertisau fault (Eisbacher and Brandner, 1996). This thrust is potentially connected with the main zone of current seismicity below the Inn valley, and therefore seismotectonic activity can be expected given the current stress regime. Ten kilometers west of the study area a joint-set parallel to cracked clasts in Late Pleistocene sediments was hypothesized to represent neotectonic activity (**Figure 1A**; Costantini and Ortner, 2013). Several other major faults occur in the study area, but neotectonic activity of these faults is not expected in the current stress regime (grey faults in **Figure 1C**) based on their position within the nappe stack (e.g., piggy-back of a younger out-of-sequence thrust) or orientation (e.g., too steep) obtained from previous detailed geological mapping (Ampferer and Ohnesorge, 1924; Ampferer, 1928; Krauter, 1967; Kilian and Ortner, 2019).

The Inn valley was struck by at least three severe and damaging earthquakes in the last 500 years, of which the Hall earthquake in CE 1670 reached M_W 5.7 ± 0.4 (**Figures 1A,C**; Stucchi et al., 2013). The source faults and focal mechanisms of these severe earthquakes and therefore also potentially active faults are unknown. Focal-depth distributions inferred from macroseismic data suggest an earthquake potential up to maximum M_W 6.5 (Lenhardt et al., 2007). This is about one magnitude step higher than the largest historically documented earthquake and involves fault dimensions which can be expected to produce surface ruptures (Stirling et al., 2002). However, so far, no surface ruptures are documented in the study area potentially due to long recurrence rates, and high erosion and sedimentation rates obliterating evidence in this mountainous region.

Lake Setting

The study area comprises the Achensee, a 6.8 km^2 large and 133 m deep lake occupying an underfilled, glacially-eroded, N-S oriented valley (**Figures 1C,D**). The lake level of Achensee at 930 m above sea level (asl) is about 400 m higher than the main SW-NE-trending Inn Valley (530 m asl) southeast of it. The formation of this inner-alpine lake basin is caused by natural damming of the elevated side valley by a rapid deposition of proglacial to periglacial sediments overlain by glacial till deposits related to the advancing Zillertal glacier from the Southeast preceding the Last Glacial Maximum ("Achensee dam", Poscher, 1994; **Figure 1C**). In the North, the lake is dammed by elevated bedrock in the valley. The natural outflow of the lake shifted from southwards to northwards through the build-up of the natural Achensee dam. Several natural and artificial (since Mid-20th century) inflows drain the steep and rocky local catchment (218 km^2) into Achensee.

Achensee is subdivided into four basins (from S to N) named Pertisau basin, Main basin, Gaisalm basin and Northern basin (**Figure 1D**). The three northern basins are divided by alluvial fan deltas, whereas the Pertisau basin and the Main basin are separated by a subaquatic landslide scarp (see *Mass-Transport Deposit Event Stratigraphy*). Since CE 1923 Achensee has been used as natural reservoir for hydropower production, which resulted in an artificial 1 m rise of the high lake level stand in summer, and seasonal lake level fluctuation of up to 11 m. Especially in the early phase of hydropower generation, these drastic lake level changes enhanced coastal erosion leading to several coastal and lake-internal landslides and additional progradation of alluvial fan deltas (Ampferer and Pinter, 1927; see also *Identification and Calibration of Off-Fault Paleoseismic Evidence*).

MATERIALS AND METHODS

Multibeam Bathymetry and Reflection Seismics

High-resolution bathymetric data of Achensee were acquired in October 2017 using a Kongsberg EM2040 multibeam echo sounder (University of Bern) operating at 300 kHz in a 1 × 1° beam-width configuration. A Leica GX1230+ GNSS receiver was used for positioning in combination with real-time kinematic corrections (RTK) provided by EPOSA (real-time positioning service Austria, www.eposa.at). Acoustic sound velocity was based on continuous monitoring and vertical velocity profiles (1–5 per day) using a Valeport MiniSVP probe. Subaqueous sound velocity ranged from 1,450 m/s at the water surface to 1,426 m/s in the deepest part. The recorded raw data were processed and manually reviewed in Caris HIPS/SIPS 9.1 software. The point cloud was rasterized using the "Swath Angle Surface" algorithm resulting in a bathymetric map with 1 m horizontal and a few decimeters vertical resolution. Bathymetric maps were created using QGIS Desktop 3.10.5 and GlobalMapper 13.

Two different seismic sources were used to image the sedimentary infill in pseudo-3D by a very dense grid of sparker source (99 km) and pinger source (133 km) survey lines (**Figure 1D**). A single-channel 3.5 kHz Kongsberg Geopulse pinger was used for several small seismic surveys in 2016–2019 and provides a theoretical vertical resolution of ~10 cm. The pinger was mounted on an inflatable cataraft, which was attached to a working boat of the local fishery. Survey speed was kept constant at 6–7 km/h. The incoming seismic data together with the GPS positioning (±5 m accuracy) were digitally recorded using the Coda Octopus GeoSurvey software. An intermediate frequency (0.8–2.0 kHz) "Centipede" multi-electrode sparker source (Ghent University) operating at 400 J was used in a seismic survey in 2017 and provides ~25–50 cm theoretical vertical resolution. A single-channel streamer equipped with ten hydrophones was used as receiver for the sparker survey. Both the sparker and streamer were towed by the research vessel "Luna" of the Research Department for Limnology, Mondsee (University of Innsbruck). A bandpass filter (0.2–2.3 kHz) was applied for quality control during the survey and the signal was digitally recorded as SEG-y data. Erroneous trace values were removed through a despiking algorithm. Seismic interpretation was done in IHS Markit Kingdom Suite 2018 where a bandpass filter of 2.0–6.0 kHz and 0.2–1.0 kHz was applied for better visualization of the pinger and sparker data, respectively.

Seismic stratigraphic units are defined based on seismic reflection characteristics, seismic facies and unit geometry following the terminology of Mitchum et al. (1977). In particular, we identified the typical seismic facies and geometry of lacustrine mass-transport deposits (MTDs; Sammartini et al., 2019) and mapped their spatial and stratigraphic distribution (e.g., Schnellmann et al., 2006) in the sedimentary infill of the Pertisau basin and the Main basin. The Northern and the Gaisalm basins were excluded from this study, because there are less than 3 ms seismic penetration in the Northern basin and the sedimentation in the Gaisalm basin is strongly influenced by episodical detrital input from large fan deltas (**Figure 1D**). We evaluate whether the spatio-temporal distribution of MTDs in Achensee can be used as off-fault paleoseismic evidence following the concept of tracing multiple MTDs on single stratigraphic levels which are directly overlain by a (mega)turbidite. This specific depositional signature hints at a coeval triggering of subaqueous mass-wasting and can potentially be related to severe seismic shaking (Schnellmann et al., 2002; Strasser et al., 2013; Moernaut, 2020).

We further identify non-sedimentary and subvertical reflection patterns offsetting the sedimentary infill, hereafter generically termed "subaqueous fault" independent of its formation or causal processes. Strong reflections are used as stratigraphic control horizons and for measuring the fault throw on the seismic lines defined as vertical displacement (positive = up; negative = down) of one fault block in respect to the other. Fault throw measurements were conducted on multiple stratigraphic levels in order to test for repeated activity along a fault (Cartwright et al., 1998). Based on the stratigraphic level of upper fault termination, different generations of fault activity are defined and mapped throughout the seismic data. A constant sound velocity of 1,500 m/s was assumed for time-depth conversions of the fault throw measurements and the creation of MTD distribution and -thickness maps. Such acoustic velocity is in agreement with results derived from multi-channel seismic-reflection data on Holocene lake sediments in glacigenic basins (Pinson et al., 2013). As pre-Holocene lacustrine strata may be more compacted and exhibit slightly higher acoustic velocity, the fault throws in the lower parts of the stratigraphy might be slightly underestimated.

Sediment Core Analyses and Event Dating

Sediment cores up to 11 m length were retrieved in the Pertisau- and Main basin using the coring platform ARARAT equipped with a modified Kullenberg-type piston coring system (ETH Zürich; Kelts et al., 1986). In addition, short cores up to 1.5 m length located near or at the piston coring locations were retrieved in 2017 and 2018 using a short gravity coring system with sliding-hammer action. All sediment cores were scanned for X-ray computed tomography (CT) using a Siemens SOMATOM Definition AS at the Medical University of Innsbruck with a voxel size of 0.2 × 0.2 × 0.3 mm. P-wave velocity, gamma-density at 0.5 cm interval on whole-round cores and magnetic susceptibility (Bartington MS2E) at 0.2 cm interval on split cores were obtained using a GEOTEK Multi Sensor Core Logger at the Austrian Core Facility of the University of Innsbruck (ACFI). Split cores were imaged right after core-opening using a Smartcube Camera Image Scanner (ACFI). Lithostratigraphic units and sedimentary event deposits (MTDs, turbidites) were identified macroscopically in combination with CT- and bulk density data. Unique sediment- and density patterns were used for inter-basin core-to-core correlation. Core-to-seismic correlations are based on linking abrupt shifts in density with strong reflections and by linking units of deformed (folded) sediments in the core with mapped MTDs on the seismic profiles.

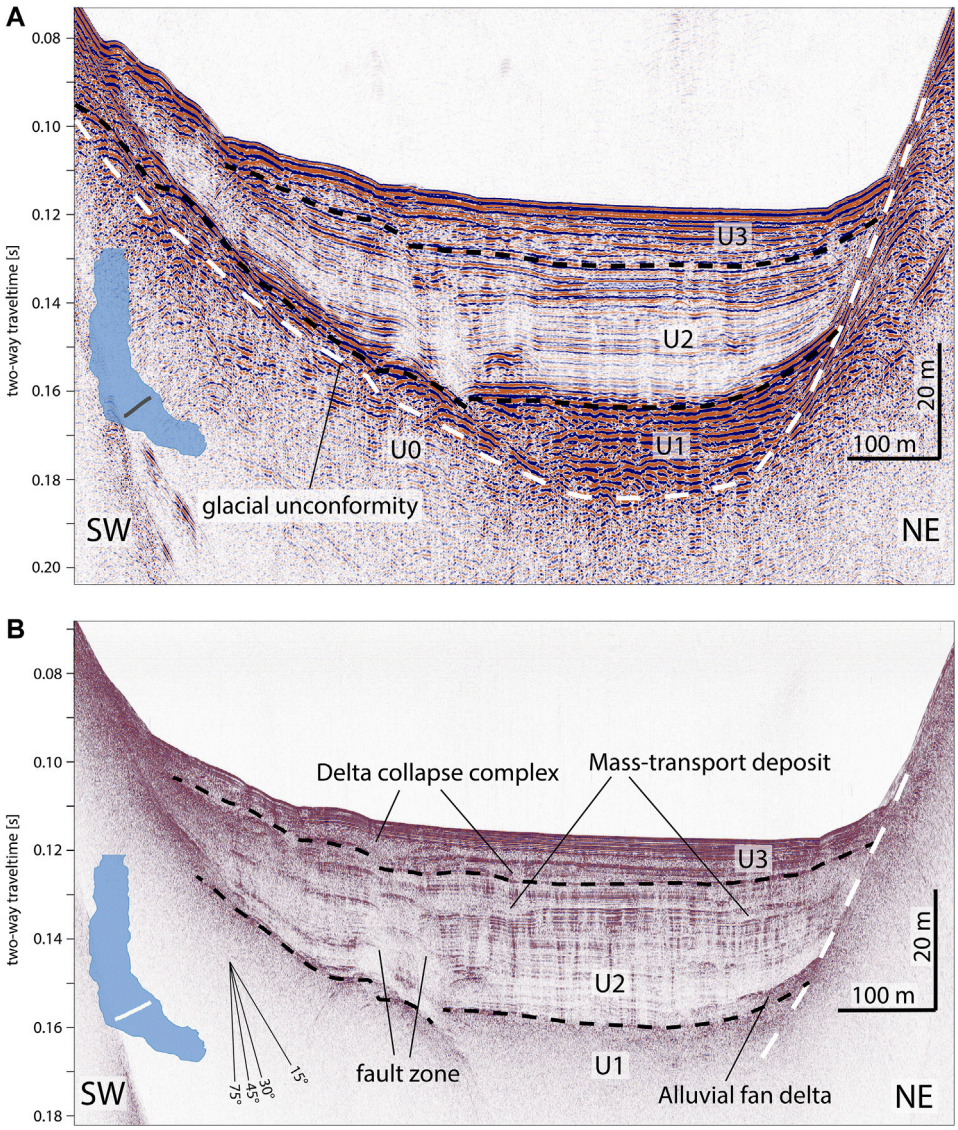

FIGURE 2 | Seismic profiles across the Pertisau basin using an intermediate-frequency sparker source **(A)** and a high-frequency pinger source **(B)**. **(A)** The sparker profile images the whole post-glacial sedimentary infill subdivided in three seismic units (U1–U3; black dashed lines) onlapping the glacial unconformity (white dashed line). **(B)** The pinger profile accurately resolves wedge-shaped mass-transport deposits and a delta collapse complex intercalated in U2 and U3. Vertical blurred fault zones offset the sedimentary infill.

Terrestrial macro-organic remains (i.e., leaves and needles) were radiocarbon dated using accelerator mass spectrometry at the Laboratory for Ion Beam Physics at ETH Zürich. ^{14}C ages were calibrated using IntCAL20 (Reimer et al., 2020) and are reported in calibrated years before present (cal BP). Short-lived radionuclide (^{137}Cs) activities were measured at EAWAG (Dübendorf, Switzerland) with CANBERRA and Princeton 146 Gamma-Tech germanium well detectors. Short-lived radionuclide activities and radiocarbon dates derived from short cores were projected via core-to-core correlation to the long cores ACH19-L3 and ACH19-L7 (**Supplementary Figure S1**). Sedimentary event ages were determined in both basins on the master cores ACH19-L3 and ACH19-L7 based on Bayesian age-depth modelling using the Bacon v2.4 software package in R (Blaauw and Christen, 2011). Several ^{14}C dates are objectively assigned as outlier ages by evaluating preliminary age-depth modelling runs and are therefore excluded for the final age-depth modelling. For the age-depth model, all instantaneous event deposits > 1 cm thickness are removed resulting in an event-free sediment depth.

RESULTS

Seismic Stratigraphy

The intermediate-frequency (0.8–2.0 kHz) sparker source provides information on the whole sedimentary infill and penetrates down to

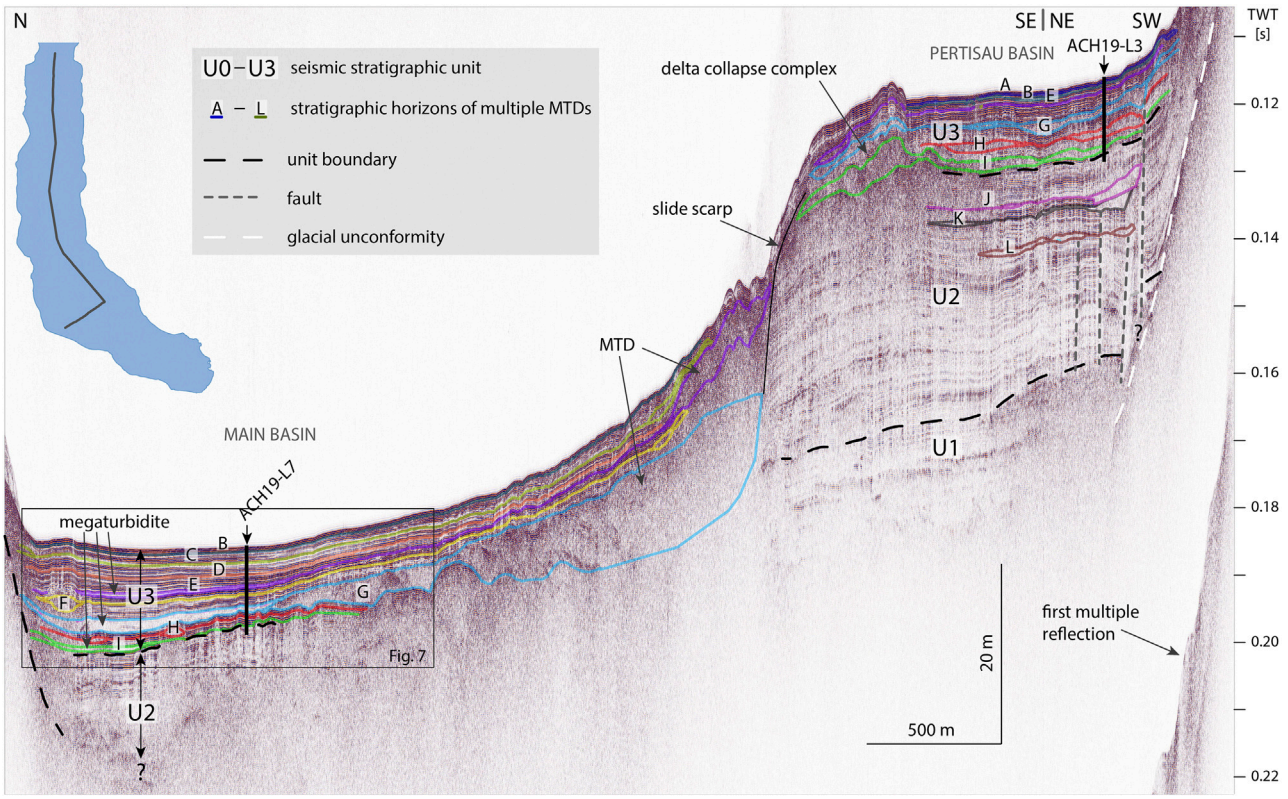

FIGURE 3 | Pinger seismic profile across and along the Pertisau basin towards the long axis of the Main basin showing comparable seismic units U2 and U3 and event horizons (A–L) correlated by core-to-core-to-seismic correlation (see *Core-to-Core and Core-to-Seismic Correlation*). The basins are subdivided by a slide scarp corresponding to the large MTD of event G. The depocenter of the Main basin contains three megaturbidites within event horizons E, G and I. Map inset shows the trend of the seismic profile. Vertical black lines display projected depth of core ACH19-L7 and ACH19-L3 from the Main basin and Pertisau basin, respectively (**Figure 9**).

~55 m depth in the Pertisau basin (**Figure 2A**), whereas the high-frequency (3.5 kHz) pinger source images the infill in high-resolution down to ~35 m depth in the Pertisau basin (**Figure 2B**).

Seismic stratigraphic analyses in the Pertisau basin reveals three main seismic units (U1-U3) deposited above a truncated substratum (U0; **Figure 2A**). U0 has low- to intermediate-amplitude, inclined and semi-continuous reflections. It is truncated by an asymmetrically bowl-shaped unconformity, which forms the basal surface on which U1-U3 are deposited. U1 has high-amplitude reflections varying from more chaotic at the bottom to semi-continuous towards the top. U1 is mainly located in the deepest part of the basin and its reflections onlap the basal unconformity. The onlaps of U1 are clear on the NE slope, whereas on the SW slope these are difficult to identify due to hyperbolic reflection patterns. The top of U1 defines the acoustic basement in the pinger data (**Figure 2B**). U2 is characterized by alternating low- to intermediate-amplitude seismic facies with continuous reflections onlapping the basal unconformity towards the slope of the basin. Locally, wedge-shaped, high-amplitude bodies with down-lapping reflections occur in the lower part of U2 near the basin slope break (**Figure 2B**). Similar to U1, onlaps are more distinct at the NE slope, whereas on the less inclined SW slope the reflections partly show onlap but also a more draping configuration. U3 generally exhibits continuous high-amplitude reflections with draping character.

In contrast to the Pertisau basin, seismic data in the Main basin only covers U3 and the upper part of U2 (**Figure 3**). The upper part of U2 and most of U3 contain numerous MTDs (stratigraphic horizons A-L in **Figure 3**) located at the slope-basin transition. The MTDs occur in both the Main- and Pertisau basin and are characterized by a positive relief with basin-ward thinning geometry and a chaotic low- to intermediate-amplitude seismic facies (**Figure 2B**). Some MTDs are directly overlain by semi-transparent seismic bodies with ponding geometries and a smooth top surface in U3 of the Main basin and are interpreted as megaturbidites resulting from large subaqueous mass wasting (**Figure 3**; see *Mass-Transport Deposit Event Stratigraphy*; e.g., Schnellmann et al., 2006).

The Pertisau basin seismic-stratigraphic unit succession closely compares to the type stratigraphy of glacigenic lake sequences as established for other alpine and peri-alpine lakes (Van Rensbergen et al., 1998; Ndiaye et al., 2014; Daxer et al., 2018; Fabbri et al., 2018). Accordingly, we interpret the basal unconformity as a glacially scoured valley into a sedimentary succession (U0) deposited before the Last Glacial Maximum. U1 is interpreted as a rapid and coarse sediment infill ("glacial outwash") below or directly in front of the glacier in the

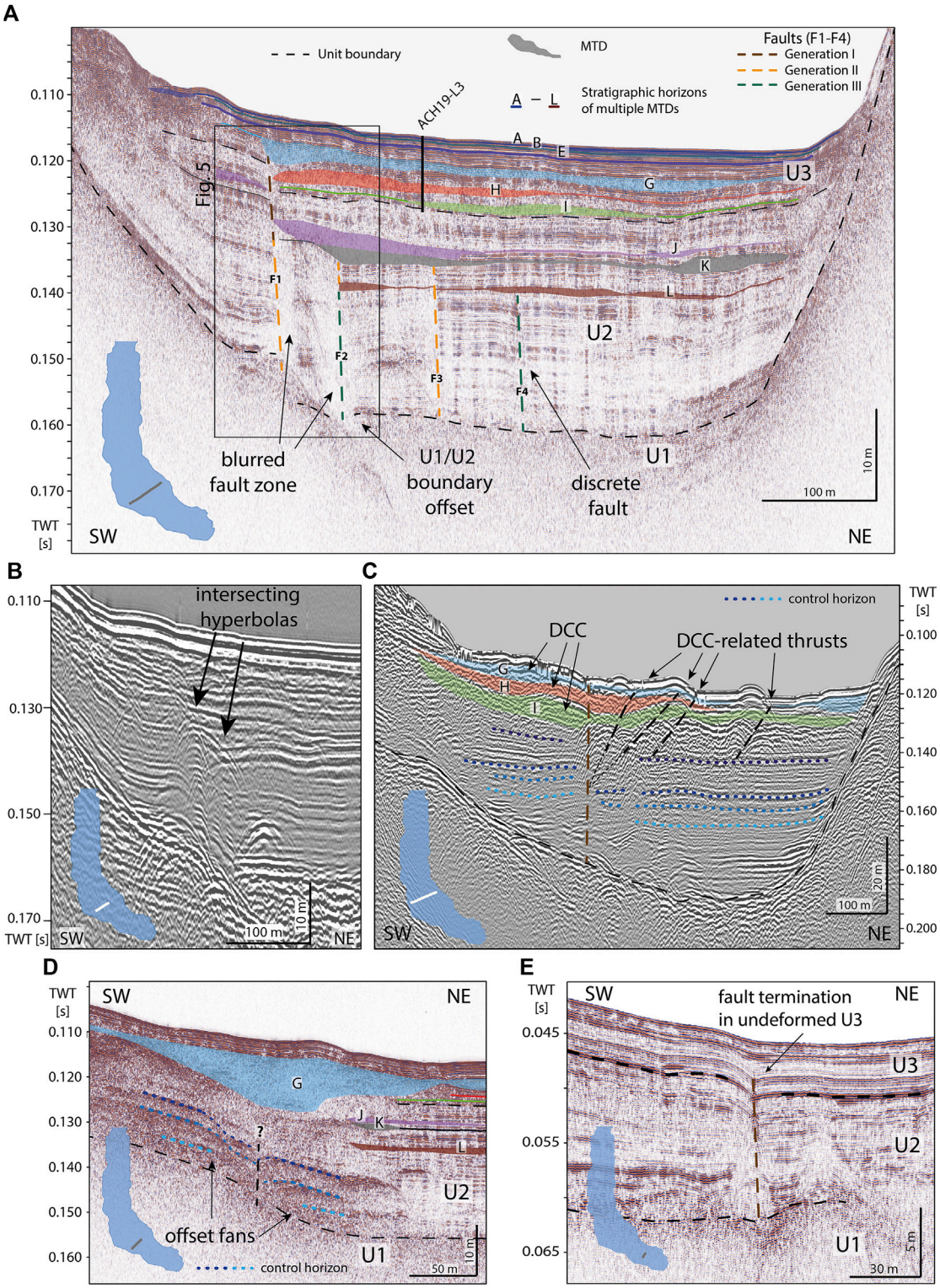

FIGURE 4 | Seismic profiles across the Pertisau basin with interpretation of both on-fault and off-fault paleoseismic evidence. Locations of the seismic profiles are indicated by the respective inset. **(A)** Pinger profile with four faults expressed as blurred zones or discrete offsets, which are subdivided in faulting generations I, II and III based on the stratigraphic level of their upper termination. Event horizons A-L depict stratigraphic horizons with multiple MTDs. The upper termination of fault generations I, II and III are directly overlain by MTDs of event horizons G, K and L. Vertical black line displays projected depth of core ACH19-L3 (**Figure 9**). **(B)** Fault zone expressed by intersecting hyperbolas in a sparker profile. **(C)** A blurred fault zone offsetting seismic-stratigraphic control horizons (dark- to light blue) in a sparker profile. The fault terminates

(*Continued*)

FIGURE 4 | in the delta collapse complex (DCC). Transportation and emplacement of the DCC generated deformation and thrusting of basin sediments. **(D)** Offset of fan delta deposits locally characterize the fault zone, where faulting generations could not be assigned due to missing stratigraphic control between the MTD of event horizon G and the fan delta deposits. Pinger profile. **(E)** A discrete fault terminating upwards in undeformed U3 in the shallow SE-most part of the Pertisau basin. Pinger profile.

Achensee valley, which is retreating to the SE into the main Inn valley or the Ziller valley. Moreover, a relatively minor sediment contribution to U1 may be formed by meltwater streams from retreating glaciers in the local side valleys of Achensee (e.g., upstream Pertisau; **Figure 1C**). U2 is interpreted as glaciolacustrine sedimentation with contemporaneous progradation of alluvial fan deltas in a proglacial lake setting with respect to the local glaciers. U3 represents recent open lacustrine hemipelagic sedimentation. The U2/U3 boundary is identified in core ACH19-L3 as a lithostratigraphic boundary confirming the seismic-stratigraphic interpretation (see *Lithostratigraphy*). A stack of three large and complex MTDs within U3 (**Figure 2B**) originates from the Pertisau delta and represent deposits of delta collapses, hereafter named as "delta collapse complex" (DCC). The surface expression of the DCC is also visible on the present-day bathymetric data as irregular to semi-concentric ridges (**Figure 1D**) caused by thrusting during DCC propagation and emplacement (see *Subaqueous Faults*; Sammartini et al., 2021).

Subaqueous Faults

Seismic units are not laterally continuous across the Pertisau basin due to the occurrence of sub-vertical faults offsetting the sedimentary lake infill (**Figures 2A,B**). Most of these subaqueous faults are visualized as a steep (~80°) NE-dipping to subvertical, decameter broad zone where seismic penetration is blurred and bordered by bent reflections (F1 and F2 in **Figure 4A**). Within the blurred zones, faint hyperbolic reflections occur that are better visible in sparker profiles (**Figure 4B**). Juxtaposed half or incomplete hyperbolas occur in both directions and are intersecting, suggesting an abrupt termination of strata on both sides of the fault. A second expression are narrow, discrete subvertical faults (F3 and F4 in **Figure 4A**), where reflections are bent towards the faults and total vertical offsets are minor. Besides these subvertical fault types, inclined thrusts occur below the DCC (**Figure 4C**) creating pronounced ridges of up to 2 m height on the lake floor. The two northeastern DCC-related thrusts sole in undeformed strata of U2 (dark blue dotted horizon in **Figure 4C**), whereas the lower contact of the two southwestern DCC-related thrusts is unclear and potentially connects with the sub-vertical blurred fault zone (dashed brown line).

The lowermost extent of subvertical faults that can be identified on pinger profiles is located at the top of U1. The faults can also not conclusively be traced further down on sparker profiles (**Figures 2A**, **4C**), probably due to non-continuous reflections of U1 and U0. The faults terminate at three specific stratigraphic levels, which are also marked by the presence of MTDs labelled G, K and L (**Figure 4A**; see details in *Mass-Transport Deposit Event Stratigraphy*) implying fault activity during at least three different events. Therefore, the faults are assigned to fault generations I, II and III from young to old and colored brown, orange and green in **Figure 4A** and all subsequent figures, respectively. There is no observational evidence, neither in seismic profiles nor in bathymetry, that one of these faults offsets the topmost lacustrine strata younger than the fault generation I. Towards the southern Pertisau basin an alluvial fan delta in the lower U2 is present on the SW slope resulting in

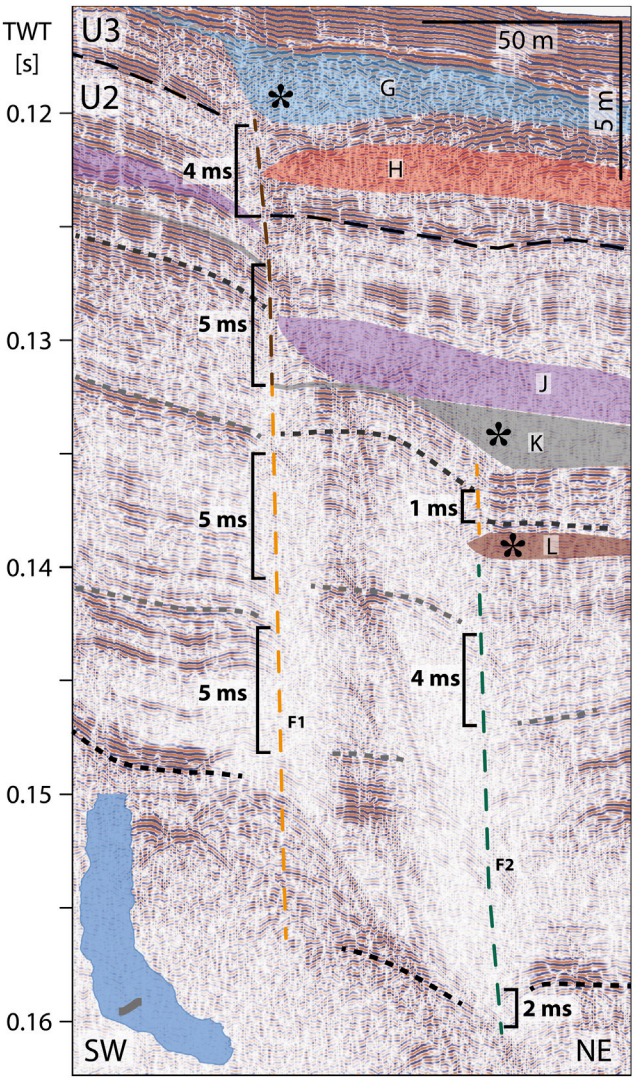

FIGURE 5 | Zoom of **Figure 4A**. Subaqueous faults of different generations are directly overlain by MTDs indicated by stars. Fault throw (ΔT) is measured using seismic-stratigraphic control horizons (narrow dashed lines). Faults are colored based on their upper termination in faulting generation I, II and III (color code in **Figure 4A**). Stratigraphic control horizons are shown as narrow dashed lines. Note the fault growth sequence along both faults and the reversal of fault throw of the F2 fault. Map inset in lower left shows position of the pinger profile.

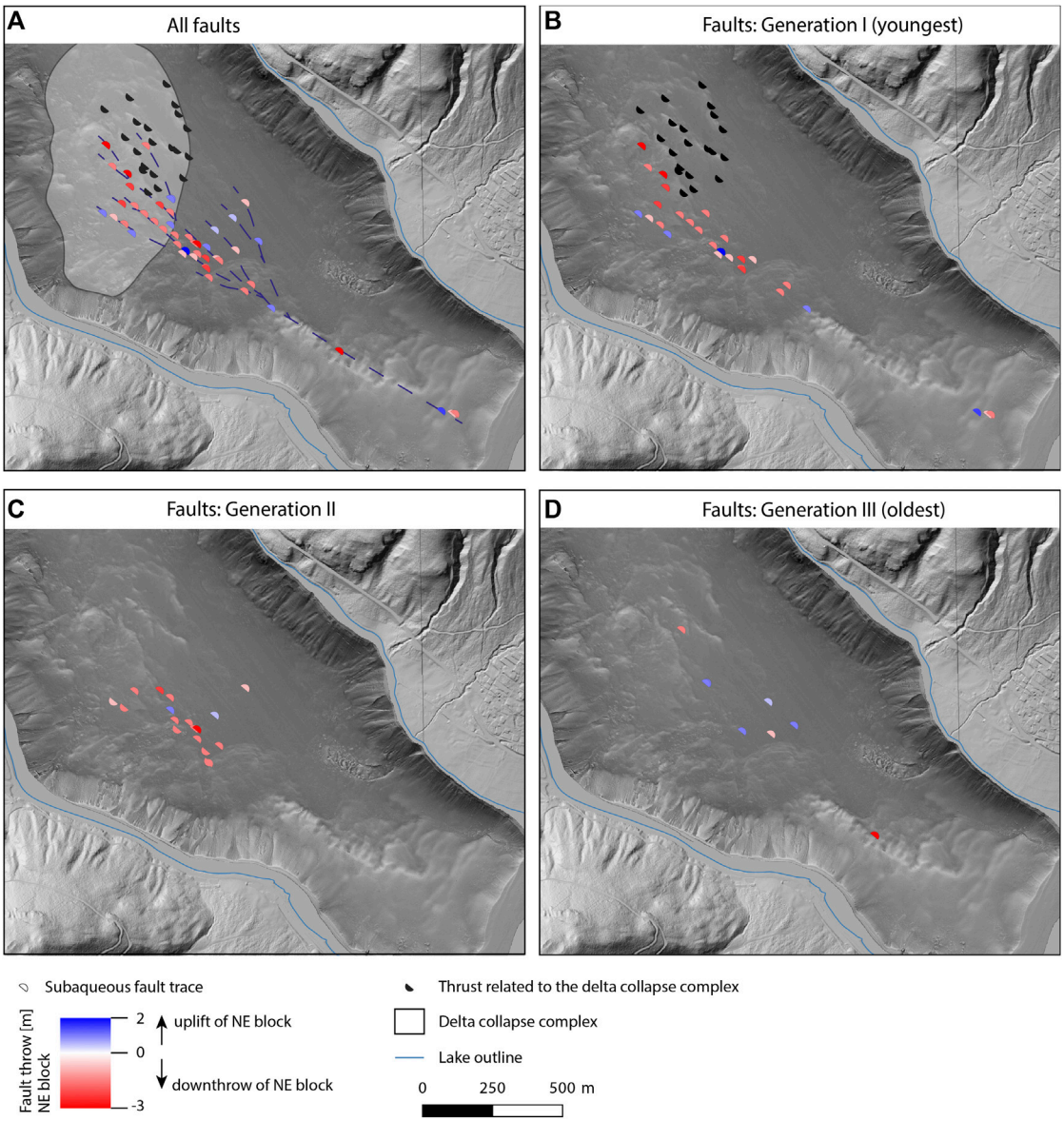

FIGURE 6 | (A) Subaqueous faults trace maps in the Pertisau basin colored with their respective fault throw, where a negative value defines downthrow of the NE block in respect to the SW block and vice versa for positive values. Thrust faults related to the emplacement of the delta collapse complex (DCC) are colored black. A potential interpretation of interconnected fault traces is shown by dark-blue dashed lines. The individual fault generations I-III are distinguished in **(B–D)** based on the upper termination of the subaqueous faults in the stratigraphy (see also **Figures 4A**, **5**).

a different and less distinct fault expression (**Figure 4D**). The stratigraphic offset is visible on the basis of the different fan wedges (indicated by blue dotted horizons) showing relative downthrow of the NE block. In between the alluvial fan deltas and the blue-colored MTD (labelled G in **Figure 4D**), reflections are rather weak, discontinuous and cannot be traced across the fault. This excludes a conclusive interpretation of its upper termination and therefore has not been assigned to any fault generation. In the SE-most part of the Pertisau basin (**Figure 4E**), where water depth is only about 30 m and seismic units U2 and U3 are condensed, a discrete fault is present with a relative downthrow of the NE block. Reflections are bent towards the fault and intersect at the fault location. The fault clearly offsets the U2/U3 boundary, whereas it terminates within U3 (**Figure 4E**) in which its morphological expression is partly leveled out by the overlying undeformed sediment sequence. Therefore, we assign this fault trace in **Figure 4E** as a potential generation I fault. However, presence of older fault activity, which is not visible due to low sedimentation rates in this shallow area, cannot be excluded.

Some faults exhibit variable vertical fault throws (ΔT), which are defined as vertical displacement of the NE block in respect to the SW block (**Figure 5**). Upward decreasing fault throw, as

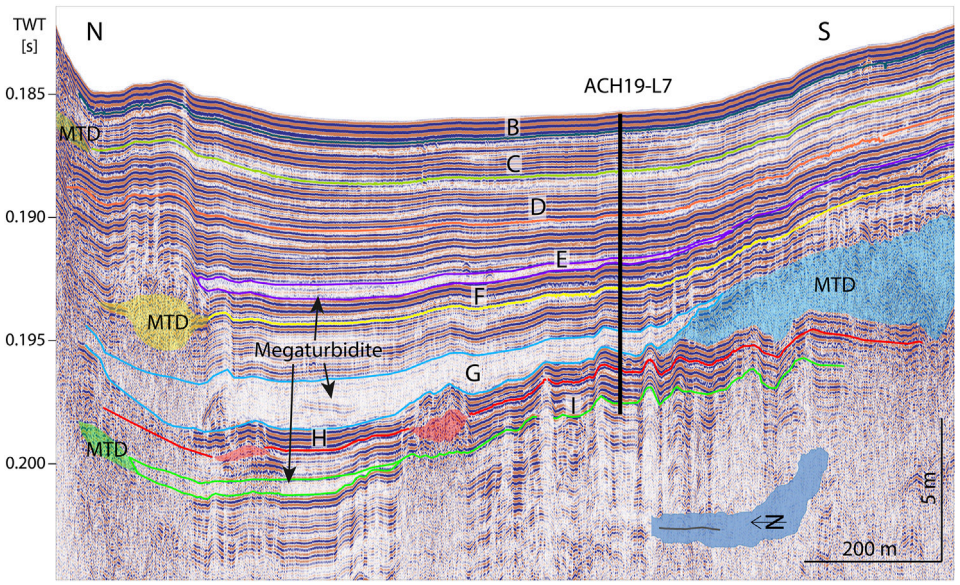

FIGURE 7 | Pinger profile along the Main basin (zoom of **Figure 3**). The Main basin contains a complete record of event horizons (B–I) with multiple MTDs. In event horizons G and I, MTDs are directly overlain by megaturbidites indicating their cogenetic formation. Vertical black line displays projected depth of core ACH19-L7 (**Figure 9**). Map inset indicates location of seismic profile.

present in the upper part of both faults in **Figure 5** indicates fault growth in multiple phases (Cartwright et al., 1998; Bouroullec et al., 2004; Barnes and Pondard, 2010). Accordingly, the F1 fault is considered active during generations I and II, whereas activity of the F2 fault is assigned to generations II and III. The considered fault throws indicate relative downthrow of the NE block. In contrast, the lower part of the F2 fault shows relative uplift of the NE block and thus throw reversal along the same fault. This is a potential indication for strike-slip movement (Zalan, 1987; Barnes and Audru, 1999) during which an apparent vertical offset in profile view can be generated by horizontally offsetting inherent basin morphology. In map view, all subaqueous fault traces—independent of their assigned fault generation—are aligned in SE to NW direction roughly parallel to the main axis of the Pertisau basin (**Figure 6**). The mapped fault traces are more discrete in the SE part of the basin and splay up to several sub-parallel fault branches towards the NW (dashed lines in **Figure 6A**). In the NW-most part, only a single to maximum two faults can be mapped below the DCC due to limited depth penetration of the acoustic signal and the deformed basin sediments caused by the propagation and emplacement of the DCC. The thrusts related to the DCC form a peculiar succession of NW-SE oriented ridges semi-parallel to the other faults. This semi-parallel configuration of DCC-related faults is different from the typical arcuate-shaped frontal thrusts of delta collapses observed in other Alpine lakes (Hilbe et al., 2014; Strasser et al., 2020; Sammartini et al., 2021). In a generation-based distinction of fault traces (**Figures 6B–D**), the youngest (I) and oldest (III) generations clearly indicate the overall SE-NW trend, whereas the fault traces of generation II show two outliers to this general trend with low fault throw values. Negative fault throw measurements can be traced over several adjacent profiles and overall indicate a downthrow of the NE block with maximum total vertical offsets of circa -3 m (**Figure 6A**). Positive fault throws up to 2 m are documented, but appear to occur locally on single profiles.

Based on the individual observational evidence with respect to offsets in the glaciolacustrine-to-lacustrine stratigraphy over numerous seismic profiles and the coherent alignment of fault traces, we interpret that the individual mapped fault traces are interlinked and altogether describe a SE-NW striking subaqueous fault zone (**Figure 6A**). The co-existence of mainly relative downthrow of the NE block with only locally occurring uplift of the NE block can be explained by a strike-slip fault motion accompanying the normal faulting of the NE block. Based on the observational evidence of a fault growth sequence with three faulting generations, we suggest that the sedimentary succession of Achensee recorded on-fault paleoseismic evidence for at least three times in Late-Glacial to Holocene times.

Mass-Transport Deposit Event Stratigraphy

The identified MTDs are characterized by low- to intermediate-amplitude reflections of chaotic and basin-ward thinning seismic bodies with a positive relief (**Figures 2–4**, **7**) and occur in both investigated basins. Besides the peculiar occurrence of a DCC in the Pertisau basin (see *Seismic Stratigraphy*), an extraordinary large MTD (~1.5 km long and up to 12.5 m thick) covers most of the Main basin (MTD in event horizon G in **Figure 3**). This MTD is derived from the

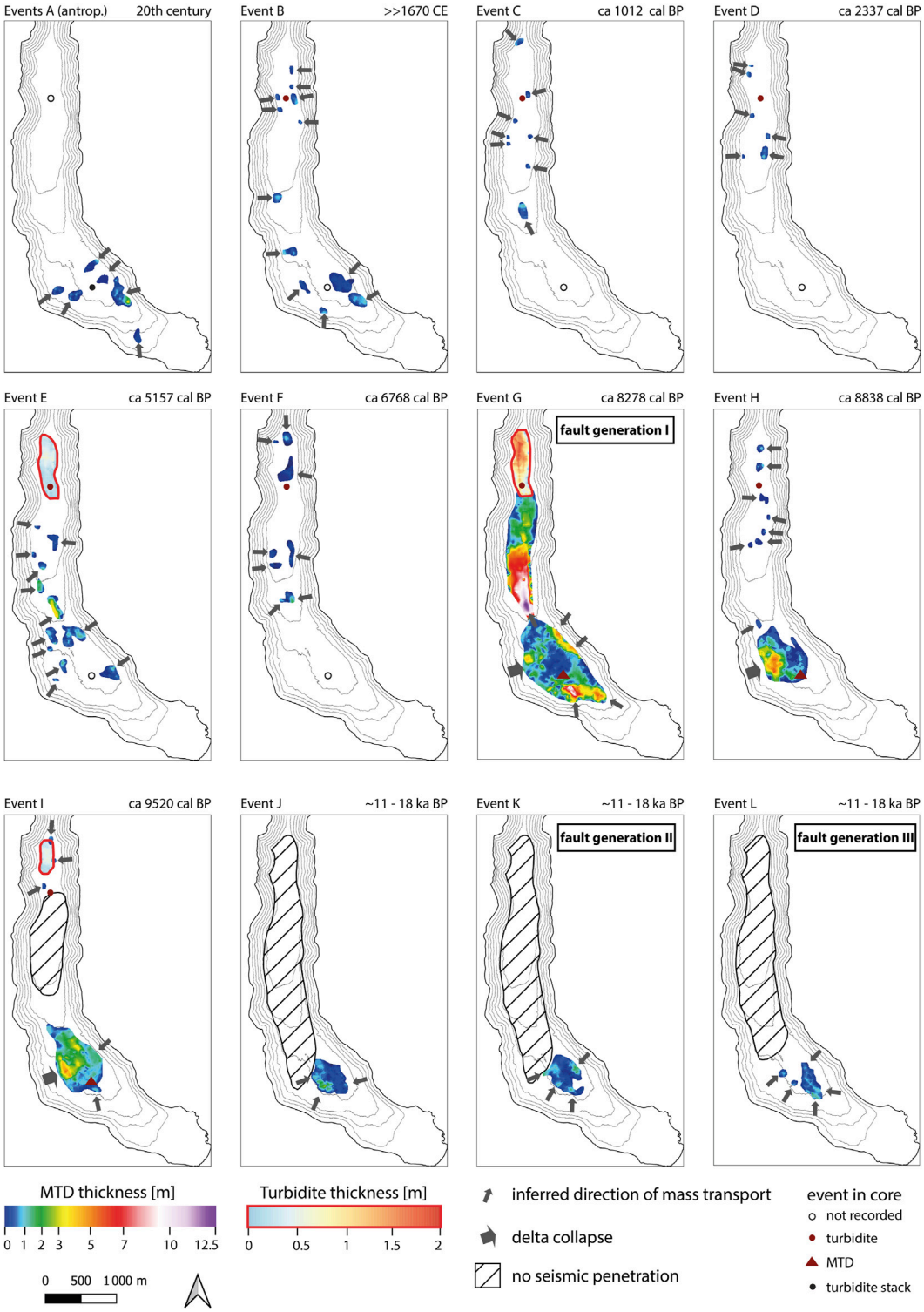

FIGURE 8 | Distribution and thickness maps of MTDs and megaturbidites of seismic-stratigraphic event horizons A-L. Symbols and color code of the coring sites provides information on the sedimentary imprint of the event in the cores. See main text for interpretation and dating of the individual events.

lake-internal slope dividing the Pertisau basin from the Main basin, which contrasts to all other MTDs that originate from lateral basin slopes. Its slide scarp truncates U2 and U3 reflectors of the Pertisau basin, which suggests that this MTD is caused by a lake-internal basin collapse, where parts of the Pertisau basin sequence failed and were transported into the

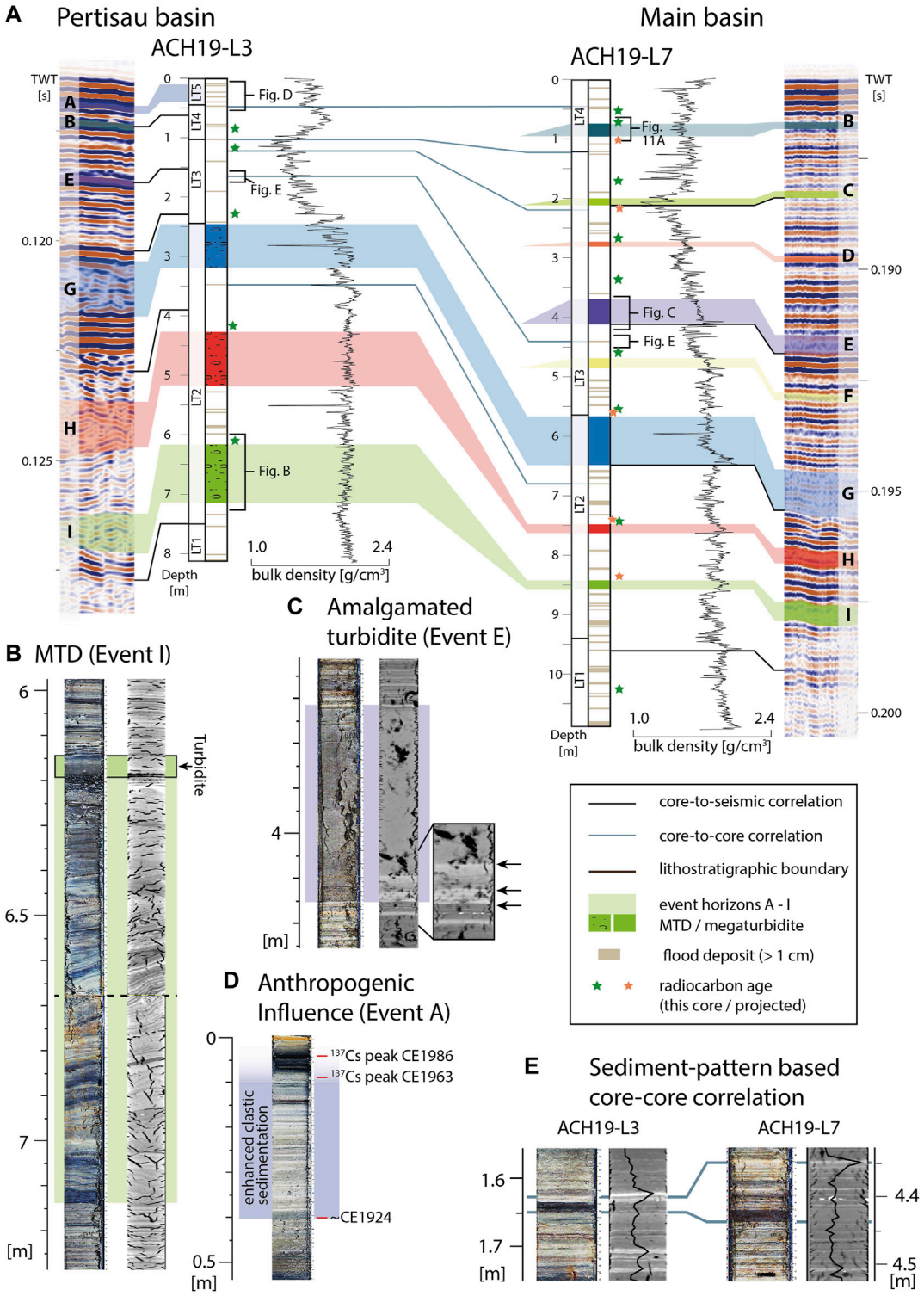

FIGURE 9 | Core data from the Pertisau basin (core ACH19-L3) and the Main basin (core ACH19-L7). **(A)** Correlation of seismic-stratigraphic event horizons A-I within the two basins is based on this core-to-core correlation using distinct marker horizons (blue lines), event deposits (MTDs and megaturbidites), density data within the different lithostratigraphic types (LT 1–5) and verified by ^{14}C dates in the cores. Core images and CT data are shown in **Supplementary Figure S1**. Core images and CT data of the different lithotypes and event deposits are displayed in **Supplementary Figures S2, S3**, respectively. Note that only events G, H and I are recognizable in both cores. **(B)** Core image and CT scan of a MTD showing folded and distorted strata, shear zones and a turbidite on top. **(C)** Core image and CT scan of an amalgamated turbidite consisting of ~3 individual sedimentary pulses (black arrows; event E). Each of these pulses has an internally homogeneous character. This

(*Continued*)

FIGURE 9 | amalgamated turbidite corresponds to the megaturbidite interpreted in seismic data (**Figure 7**). **(D)** Highly-clastic sedimentary facies (LT 4) with stacks of turbidites occurs in the upper part of ACH19-L3, and is interpreted as the result of anthropogenically-caused shoreline erosion starting at CE 1924. **(E)** Example for the sediment pattern-based core-to-core correlation. Note that the strata of the Pertisau basin (ACH19-L3) is condensed in respect to the deep basin (ACH19-L7). Lighter shades on the CT image indicate higher CT-density.

Main basin, similar to observations on basin collapses in some fjord settings (Bellwald et al., 2016). Moreover, three megaturbidites occur in the depocenter of the Main basin (**Figure 7**). These are characterized by a semi-transparent seismic facies and clear ponding geometries. A direct onlap of megaturbidites at MTDs indicates a cogenetic occurrence (event horizons G, I in **Figure 7**).

The slide scarp and thick MTD of the basin collapse disturbed the natural stratigraphic transition from the Pertisau basin to the Main basin and thus, prohibit inter-basin correlation based on tracking of continuous reflections on seismic data. Therefore, we made an inter-basin correlation of event horizons based on a core-to-core-to-seismic correlation. First, a core-to-core correlation was carried out using distinct sedimentary layers and common lithostratigraphic facies, which was verified by radiocarbon ages from both basin sequences. Afterwards, each core was correlated to seismic data to obtain a lake-wide dated event stratigraphy (see *Core-to-Core and Core-to-Seismic Correlation* for further details). In the Pertisau and Main basin we distinguished 12 event horizons (A to L; from young to old) each comprising 3–12 coeval MTDs (**Figure 8**). Besides several event horizons containing MTDs in both basins (B, E, G, H, I), event horizons C, D, F and A, J-L only show MTD occurrence in the Main basin or the Pertisau basin, respectively (**Figures 3**, **8**). The lack of MTDs is mainly caused by missing seismic penetration in the deeper parts of the Main basin and probably due to lowered sedimentation rates in the Pertisau basin (see discussion in *Natural and Methodological Factors Influencing the Lacustrine Seismograph*).

MTDs of event horizons G, K and L directly overlie the fault plane in the downthrown block where they partly level out the fault throw (**Figures 4A**, **5**). This suggests that the deposition of MTDs was coeval or occurred shortly after the faulting of the lacustrine strata. The MTDs themselves are overlain by undisturbed and draping reflections representing background sedimentation. Event horizon K is an exception, as it is directly overlain by another MTD of event horizon J with only little background sediment in between.

Sediment Core Data

Lithostratigraphy

The sediment cores ACH19-L3 and ACH19-L7 were recovered in the Pertisau basin and the Main basin, respectively (**Figures 1D**, **3**, **4**). Based on macroscopic identification in combination with CT data and gamma-ray density, a lithostratigraphic succession intercalated by various instantaneous event deposits can be identified (**Figure 9A**). The lithostratigraphic succession of Achensee comprising five lithotypes (LT1-5 from base to top) is defined at ACH19-L3 (**Figure 9A**, **Supplementary Figure S1**), because changes in sediment type are more pronounced in the Pertisau basin. Moreover, sedimentation in the Main basin is more influenced by clastic input of the alluvial fans resulting in more frequent and often relatively thicker intercalated event deposits in the Main basin compared to the Pertisau basin. Nevertheless, all lithostratigraphic units described below can be correlated to the Main basin core ACH19-L7 (**Supplementary Figure S1**). A documentation with core image and CT data of all lithotypes is provided in **Supplementary Figure S2**. LT1 (8.10–7.5 m) consists of ochre to brown laminated, mixed hemipelagic-detrital carbonate mud intercalated by <2 cm thick, brown, turbidites with abundant, sand-to-silt size detrital carbonates and terrestrial macro-organic remains. Density ranges between 1.9 and 2.1 g/cm^3 showing a slight decrease towards the top. The transition between LT1 to LT2 is defined by a distinct color change to grey. The intercalated turbidites in the basal LT2 have less common terrestrial macro-organic remains, and are generally thinner and contain smaller grainsizes compared to LT1. LT2 (7.5–2.4 m) is generally characterized by grey, fine-laminated hemipelagic-detrital mud with sparse occurrence of diatoms. Intercalations of turbidites vary in color from light-grey to brown reflecting the amount of entrained organic content and vary in thickness from a few mm to 3 cm. Moreover, three MTDs occur within LT2 (see *Event Deposit Types*). Density is rather constant within LT2 between ~1.6 and ~2.2 g/cm^3, but has some negative outliers due to sediment cracks and more variability caused by the MTDs. The transition to LT3 is marked by the top of the blue colored MTD (**Figure 9A**). LT3 (2.4–1.0 m) is a diverse lithotype but generally characterized by less clastic and increasing organic-rich sedimentation. LT3 is divided into two different subtypes, which together follow a generally decreasing density trend (1.2–1.7 g/cm^3) towards the top. The basal subtype (2.4–2.2 m) consists of grey, sub-mm, faintly laminated carbonate mud with only few <5 mm thick turbidites. The upper subtype (2.2–1.0 m) is characterized by light grey to black, very faint thin bedded carbonate mud with sparse occurrence of <1 cm thick turbidites. Especially the top part predominantly contains black beds and low density, indicating a more organic-rich sedimentation. LT4 (1.0–0.4 m) is characterized by ochre- to brown, laminated carbonate mud with occurrence of diatoms and abundant presence of 1–2 cm thick turbidites. In contrast to LT3, the density pattern of LT4 is generally increasing from bottom to top with values between 1.2 and 1.8 g/cm^3. LT5 (0.4–0.0 m) contains abundant light-grey <2 cm thick turbidites forming a turbidite stack. The upper 12 cm are characterized by black- and ochre-colored sediment likely representing the common lake eutrophication in the mid- to late 20th century in the Alps and subsequent restoration by installation of a ring canalization in CE 1991 (Sossau, 1995). LT5 is the only lithotype which is not present in ACH19-L7 in the Main basin, where LT4 extends to the lake bottom.

Event Deposit Types

Light-grey to brown-colored turbidites with normal grading from sand to silt and a thickness ranging between a few mm to

maximum 5 cm occur abundantly within the sedimentary succession of both cores. We interpret this type of event deposit as river flood- or debris flow-induced turbidites in accordance with sedimentological results obtained in similar lacustrine settings (e.g., Irmler et al., 2006; Gilli et al., 2013; Wilhelm et al., 2013). This abundant occurrence of debris flow- and flood-induced turbidites is supported by the presence of numerous fan deltas at the mouths of small rivers or creeks draining small and steep catchments. This indicates a high sediment availability in the catchment and effective sediment transport during high precipitation events.

In ACH19-L3 three event deposits stand out with thicknesses of 0.6–1.3 m, which are characterized by folded and distorted layers and by internal shear zones creating angular unconformities of sediment packages (**Figure 9B**, **Supplementary Figure S3**). We interpret this type of event deposit as MTDs in accordance with observations in similar lacustrine settings (cf., Strasser et al., 2013). In core ACH19-L7 of the Main basin, eight event deposits each characterized by an amalgamated turbidite were identified in the sedimentary succession (**Figure 9A**, **Supplementary Figure S3**). Each amalgamated turbidite comprises several sedimentary pulses and a fine-grained top (**Figure 9C**). The deposits of the individual sedimentary pulses differ in subtle changes in color or CT-density and can show a thin normal grading at the base in addition to an overall homogeneous character. An amalgamated turbidite may indicate coeval failure of different subaqueous slopes and has been previously used as earthquake proxy in other lacustrine settings (Van Daele et al., 2017).

Core-to-Core and Core-to-Seismic Correlation

The occurrence of lake-wide distinct marker layers together with comparable sedimentary lithostratigraphic units on both cores allow inter-basin correlation of cores ACH19-L3 and ACH19-L7 (**Figure 9E**, **Supplementary Figure S1**). As a result, three amalgamated turbidites in the core ACH19-L7 correlate with the three outstanding MTDs in core ACH19-L3 and can be assigned to event horizons G, H and I. In contrast, amalgamated turbidites of event horizons B–F in ACH19-L7 do not occur in core ACH19-L3 in the Pertisau basin. Different thicknesses of lithostratigraphic units in the two cores indicate spatially varying sedimentation rates before and after event G (**Figure 9A**). Whereas background sediment thickness is rather comparable in both cores below event G, post-event G sediment thickness is much smaller in core ACH19-L3 compared to core ACH19-L7. The presented core-to-core correlation, based on sediment patterns and lithostratigraphy, is supported and verified by comparable ^{14}C ages (**Tables 1**, **2**; *Age Depth Modelling*).

A core-to-seismic correlation is based on the correlation of high-amplitude reflections in the seismic data with abrupt bulk density shifts in the core data. Additionally, distinct marker units were used for the core-to-seismic correlation, such as MTDs of events G-I in the Pertisau basin or megaturbidites of events E, G and I in the Main basin (**Figure 9**). Seismic-stratigraphic event horizons J-L were not reached by the cores. Seismic-stratigraphic event horizon A in seismic data does not correlate with a single event deposit in core ACH19-L3, as is the case for the other event horizons (**Figure 9A**), but corresponds to a ~40 cm thick, highly clastic lithofacies (LT4) with abundant light-grey turbidites (**Figure 9D**).

Age Depth Modelling

Individual age-depth models of the cores are based on ^{14}C dates and ^{137}Cs peaks (**Figure 10A,B**; **Tables 1**, **2**). Lithostratigraphic changes are inserted as stratigraphic boundaries (dashed horizontal lines in **Figure 10A,B**) in the age-depth modelling process facilitating the models to abruptly shift sedimentation rates if required by the input ages. The age-depth models of the cores ACH19-L7 and

TABLE 1 | Radiocarbon ages of core ACH19-L7.

Core ID	Sample no.	Core depth (cm)	Event-free sediment depth (cm)	Radiocarbon age (a BP ± 1σ)	95% calibrated age range (cal a BP)	Material
1963	ACH18-02_18	11	11	—	CE 1963	^{137}Cs peak projected from pertisau basin core ACH18-02
ACH17-04	ETH-85084	55	42	209 ± 22	302–rec.	Needles, leaf fragments
ACH17-04	ETH-85085	29	23	190 ± 23	294–rec.	Needles, leaf fragments
ACH17-04	ETH-85086[a]	127	68	121 ± 22	267–14	Needles, leaf fragments
ACH19-L7G	ETH-108232	203	137	385 ± 22	503–327	Pair of needles
ACH19-L7F	ETH-108233	288	199	2,259 ± 23	2,342–2,157	Intact leaf
ACH19-L7E	ETH-108234	368	261	4,101 ± 24	4,807–4,454	Needle and leaf parts
ACH19-L7E	ETH-108235	475	312	5,809 ± 25	6,674–6,499	Needles
ACH19-L7D	ETH-108236	570	369	7,232 ± 26	8,169–7,968	Needle fragments
ACH19-L7C	ETH-108237	747	410	8,551 ± 27	9,546–9,487	Needle fragments
ACH19-L7A	ETH-105422	1,043	603	9,554 ± 26	11,080–10,731	Leaf

[a]*Sample excluded for age-depth modelling.*

TABLE 2 | Radiocarbon ages of core ACH19-L3.

Core ID	Sample no.	Core depth (cm)	Event-free sediment depth (cm)	Radiocarbon age (a BP ± 1σ)	95% calibrated age range (cal a BP)	Material
ACH18-02	ACH18-02_10	7	4	—	CE 1986	^{137}Cs peak
ACH18–02	ACH18-02_18	15	9	—	CE 1963	^{137}Cs peak
ACH18-02	ETH-89637[a]	40	34	831 ± 26	778–683	5x needle fragments, one leaf part
ACH18-02	ETH-89638[a]	45	37	380 ± 24	501–322	3x needles
ACh18-02	ETH-89639	91	65	157 ± 25	284 - rec.	3x needles, three leaf parts
ACH17-01	ETH-85081[a]	40	34	3,333 ± 24	3,636–3,482	Needles, leaf fragments
ACH17-01	ETH-85080[a]	87	62	1,107 ± 24	1,060–956	Needles, leaf fragments
ACH17-01	ETH-85079	125	79	1,382 ± 23	1,344–1,278	Needles, leaf fragments
ACH19-L3D	ETH-108238	244	163	7,336 ± 29	8,189–8,030	Coating of fruit and leaf, needle fragments
ACH19-L3C	ETH-108239	418	255	8,200 ± 28	9,275–9,026	Needle fragments + coating of fruit
ACH19-L3B	ETH-108240	585	316	8,396 ± 30	9,523–8,305	Many small needle fragments

[a]*Samples excluded for age-depth modelling.*

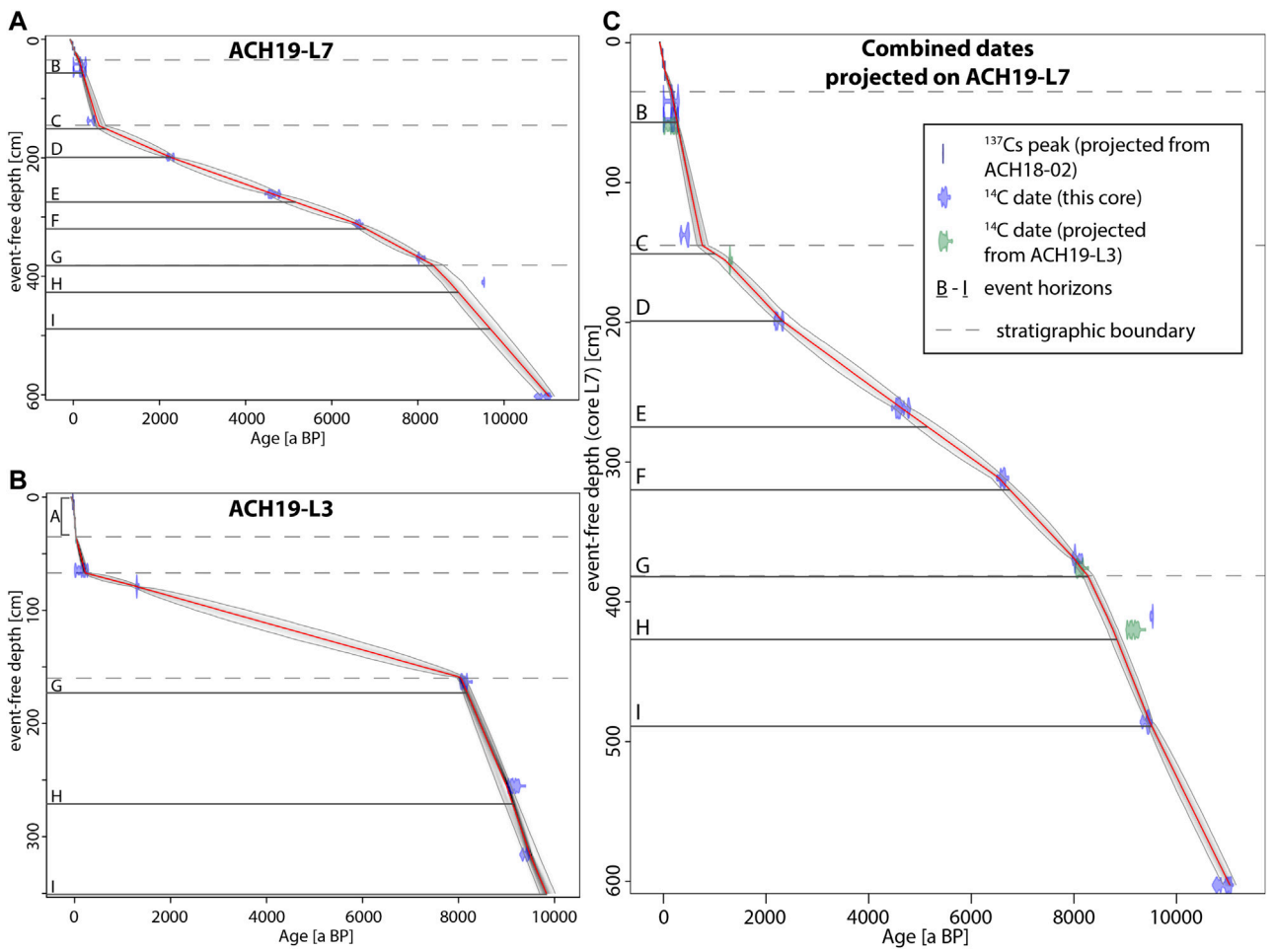

FIGURE 10 | Age-depth models of cores ACH19-L7 **(A)** and ACH19-L3 **(B)** based on combined ^{137}Cs peaks and ^{14}C dates. **(C)** Age-depth model of core ACH19-L7 contains projected ages from ACH19-L3 (colored green) based on core-to-core correlation (**Figure 9**). Mean age is indicated by red line and grey zone depicts 95% probability range. Event deposits >5 cm were identified and excluded resulting in an event-free sediment depth. Events corresponding to seismic-stratigraphic event horizons B-I are indicated by horizontal black lines.

ACH19-L3 cover the last ~10.5 and ~10 kyr, respectively, and overall show a similar sedimentation pattern. A rapid sedimentation regime occurred until ~8.3 ka BP (ACH19-L3: ~0.9 mm/year; ACH19-L7: ~2.4 mm/year), followed by a period of lower sedimentation rate until the begin of the Little Ice Age at ~450 a BP (ACH19-L3: ~0.1 mm/yr; ACH19-L7: ~0.3 mm/year) when sedimentation rates increased again until present times (ACH19-L3: ~1.5 mm/year; ACH19-L7: ~0.9 mm/year). As the core ACH19-L7 holds most cored event horizons (B-I) as distinct event deposits, it is assigned as master core for this study. Accordingly, ^{14}C dates from ACH19-L3 were projected to ACH19-L7 based on core-to-core correlation (**Figure 9**; **Supplementary Figure S1**) resulting in a more robust age-depth model (**Figure 10C**). Event ages are reported based on this composite age-depth model except for event A where the age model of ACH19-L3 is used.

Identification and Calibration of Off-Fault Paleoseismic Evidence

The youngest event horizon A, comprising multiple, coeval MTDs in seismic data while corresponding to a highly clastic lithofacies LT5 characterized by a turbidite stack, dates from CE ~1914 to ~1965 (1896–1970, 95% age range). Event horizon A is interpreted as the subaqueous expression of the historically documented enhanced shoreline erosion caused by anthropogenically induced lake level changes since CE 1924 (Ampferer and Pinter, 1927). This implies that this "event" A rather constitutes a phase of enhanced subaqueous mass wasting over a few decades, instead of a single event of coeval subaqueous failures, as was suggested by the seismic-stratigraphic analysis. Such recent human-induced mass-wasting episodes in Alpine lakes is a quite common phenomenon (Strasser et al., 2013; Daxer et al., 2019).

Event horizon B comprises twelve coeval MTDs in seismic data and an amalgamated turbidite in core ACH19-L7 (**Figures 8**, **11A**) suggesting an earthquake as causative process (c.f., Strasser et al., 2013; Van Daele et al., 2017). The age range of event horizon B (CE 1654–1737 with mean age: CE 1683, **Figure 10C**, **Table 3**) is within the dates of two severe historical earthquakes, i.e. the Hall earthquake in CE 1670 (M_W 5.7 ± 0.4) and the Innsbruck earthquake in CE 1689 (M_W 5.0 ± 0.5; Stucchi et al., 2013) and thus, potentially being caused by one of these events. The Hall earthquake may have reached a local seismic intensity (I_L) of >V½ to ~VII (EMS-98) at Achensee calculated from its magnitude value and the uncertainty on it (**Figure 11B**; Stucchi et al., 2013) in combination with an intensity prediction equation calibrated for the Swiss Alps that is also suitable for magnitudes >5.5 (Fäh et al., 2011). According to these calculations, the Innsbruck earthquake may have reached relatively lower local intensities at Achensee with I_L ~IV½–VI½. Additionally, a third historically known M_W 4.5 ± 0.5 earthquake in Schwaz (CE 1820) with calculated intensities of I_L ~IV½–VI¼ at Achensee does not seem to have a corresponding event deposit at Achensee. Therefore, we infer, that the Schwaz and Innsbruck earthquakes did not generate sufficiently-strong seismic shaking at Achensee to

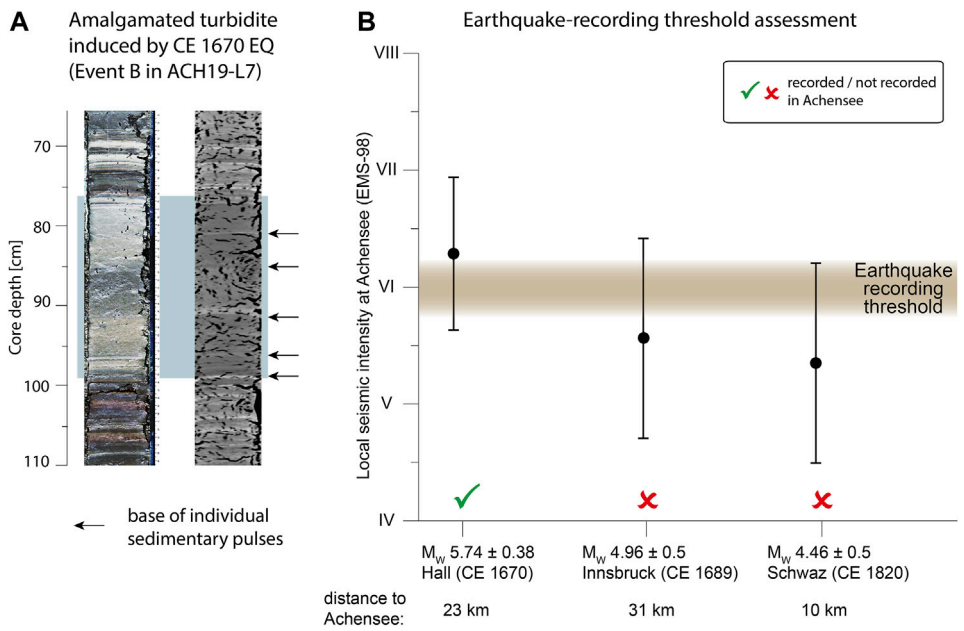

FIGURE 11 | Calibration of the earthquake imprint in Achensee. **(A)** Amalgamated turbidite consisting of five individual sedimentary pulses (black arrows) is interpreted as the sedimentary imprint of the M_W 5.7 ± 0.4 Hall earthquake (see main text for detailed description and interpretation). **(B)** Calculated seismic intensity at Achensee based on the magnitude range of historical earthquakes (Stucchi et al., 2013). An earthquake-recording threshold for Achensee at local intensity I_L ~VI results in recording the strongest historical earthquake in Hall CE 1670, but not the other two.

TABLE 3 | Event ages, paleoseismic evidence and interpretation.

Event	Age [a BP]		Off-fault evidence					On-fault evidence	Interpretation
			Seismic data			Core data			
	Mean	95% range	MTD amount	MTD volume [m³]	Megaturbidite volume [m³]	ACH19-L3	ACH19-L7		
A	1924 CE to recent		>6	16,900	—	Anthropogenic turbidite stack	—	—	Anthropogenic
B	267	213–296	12	50,000	—	—	Turbidite	—	Remote earthquake (M_W ~5.7 Hall 1670 CE)
C	1,012	849–1,164	8	15,400	—	—	Turbidite	—	Remote earthquake
D	2,337	2,213–2,578	6	10,300	—	—	Turbidite	—	Remote earthquake
E	5,157	4,930–5,394	12	165,400	50,200	—	Turbidite	—	Remote earthquake
F	6,768	6,611–6,913	8	45,600	—	—	Turbidite	—	Remote earthquake
G	8,278	8,180–8,387	5	3,404,600	189,500	MTD	Turbidite	Generation I	Local earthquake on Suzlgraben-Eben thrust
H	8,838	8,723–8,938	9	648,700	—	MTD	Turbidite	—	Remote earthquake
I	9,520	9,449–9,604	6	683,900	24,900	MTD	Turbidite	—	Remote earthquake
J	~11,000–18,000		3	111,500	—	—	—	—	Remote earthquake
K	~11,000–18,000		4	96,800	—	—	—	Generation II	Local earthquake on Suzlgraben-Eben thrust
L	~11,000–18,000		5	57,200	—	—	—	Generation III	Local earthquake on Suzlgraben-Eben thrust

leave a sedimentary imprint. Only the strongest historically known Hall M_W ~5.7 earthquake in CE 1670 was capable of inducing mass wasting at Achensee (event horizon B). By considering this positive and negative sedimentary evidence for these historical earthquakes (**Figure 11B**), we infer a seismic intensity of I_L ~VI as the threshold for generating multiple MTDs in Achensee. This is in accordance with previous studies elsewhere, where intensity thresholds for generating multiple MTDs range from I_L ~V¼–V½ in front of delta slopes in Chilean piedmont lakes and Alaskan proglacial lakes (Moernaut et al., 2014; Van Daele et al., 2019; Praet, 2020), I_L ~VI at mixed hemipelagic-clastic slopes in clastic inner-alpine lakes comparable to Achensee (Strasser et al., 2020; Oswald et al., 2021), to I_L ~VI–VII½ at hemipelagic slopes in Alpine or Chilean piedmont lakes (Monecke et al., 2004; Van Daele et al., 2015).

As the event horizons C-I each contain multiple coeval MTDs and as well correspond to an amalgamated turbidite in core ACH19-L7, we propose that these events represent paleo-earthquakes that were strong enough at Achensee to surpass the intensity threshold of VI for generating multiple MTDs, and that date back to ca. 1.0, 2.3, 5.2, 6.8, 8.3, 8.8 and 9.5 ka BP (**Table 3**). Event horizons J-L comprising multiple coeval MTDs in seismic data below the reach of the cores also potentially represent paleo-earthquakes with an age between 11 ka BP to 18 ka BP (Late Glacial times).

DISCUSSION

Quantitative Lacustrine Paleoseismology

The postglacial sedimentary infill of Achensee has recorded both on-fault paleoseismic evidence by faulting of glaciolacustrine-to-lacustrine strata and off-fault paleoseismic evidence by multiple coeval MTDs and amalgamated turbidites. Moreover, the direct superposition of MTDs (events G, K, L) on the upper termination of faults (generations I, II, III) is interpreted as co-genetic formation of on-fault and off-fault paleoseismic evidence. Although subaqueous sedimentary archives exist where on-fault evidence in seismic data is linked to seismic-induced turbidites in core data (Beck et al., 2012; Wils et al., 2018), such direct superposition of on- and off-fault evidence has rarely been documented in a subaqueous geological archive so far (Gastineau et al., 2021). Therefore, the Achensee record exhibits a unique opportunity to compare and discuss these widely used and well-established subaqueous paleoseismic methods with each other, and their implications for a better seismotectonic characterization of the region (see *Seismotectonic Interpretation*). In analogy to active tectonic regions in the marine realm (Barnes and Pondard, 2010), the sedimentary infill of Achensee potentially holds an active fault growth sequence. However, it cannot be expected that Achensee—covering only a small part of one fault in an area of several potentially active faults—contains a complete regional rupture history, as can often be derived from marine fault-growth sequence along several faults (Bull et al., 2006; Barnes and Pondard, 2010).

Multiple, coeval lacustrine MTDs can be triggered by seismic shaking independent of its source location as long as the seismic intensity at the lake site exceeds the individual earthquake-recording threshold of the archive (Monecke et al., 2004; Van Daele et al., 2015). The lake archive can document activity of any surrounding faults or also far-field sources, when fulfilling this intensity criterion. This allows reconstructing a regional paleoseismic history in places where many potentially active faults occur, such as the Alps, but identification of the active faults remains probabilistic even when adopting a multi-lake approach (Kremer et al., 2017). Therefore, by using only off-

fault paleoseismic evidence in Achensee, potential source faults would remain unknown. Above the earthquake-recording threshold, relative shaking intensities can be assessed by evaluating i) the type of the failed slope, ii) the amount of MTDs and their volume, iii) the presence of a megaturbidite, iv) evidence for postseismic landscape response, or a combination of these (Moernaut et al., 2014; Howarth et al., 2016; Van Daele et al., 2019; Oswald et al., 2021). The intensity threshold at Achensee is assessed to ~VI (EMS-98) by a combination of recording the strongest historical M_W ~5.7 earthquake in Hall CE 1670 in the form of 12 MTDs with ~50,000 m^3 total MTD volume and a 23 cm thick amalgamated turbidite in the Main basin, and not recording the other two historical earthquakes (**Table 3**, **Figure 9A**). For earthquakes E and G-L, one or more of the abovementioned quantifiable sediment parameters are exceeding the ones for the Hall earthquake. This suggests that events E and G-L generated relatively higher intensities at the lake site, and potentially represent paleo-earthquakes with higher magnitudes than the Hall CE 1670 earthquake or with epicenters closer to the lake. Accordingly, the comparison of these off-fault proxy parameters let us infer that earthquake G at ~8.3 ka BP may have had a stronger impact on the Achensee region than any of the other identified paleo-earthquakes. Event G coincides with fault generation I, interpreted as a coseismic surface rupture, and its high relative impact in terms of subaqueous mass wasting can thus be explained by the minimal distance (i.e., below the lake) between seismic source and the lacustrine slopes.

Surface ruptures as on-fault paleoseismic evidence are documented from M_W 4.9 onwards (Ritz et al., 2020) but are more commonly documented for earthquakes M_W >6.0 given a worldwide comparison (Stirling et al., 2002). As no surface ruptures were documented for the Hall M_W ~5.7 earthquake, we assume M_W ~6.0 as lower magnitude bound for the occurrence of surface ruptures in our broader study region. The maximum credible earthquake magnitude M_W 6.5 is defined for the study area based on focal depth distributions of instrumental earthquake data (Lenhardt et al., 2007). Earthquakes within the resulting magnitude range M_W 6–6.5 potentially produce surface ruptures of up to 15 km length and generate average displacements of < 1 m (Stirling et al., 2002; Brengman et al., 2019). The observed total vertical fault throws in Achensee range up to ~3 m including offsets of the three surface-rupturing generations I-III, potentially fitting the above considerations. However, application of direct fault throw-to-magnitude relationship might be misleading, because i) in the SE, where only one fault branch exists, vertical offsets are very likely apparent and modified by lateral fault motion, and ii) in the NW, where modification by the lateral motion is subordinate (see *Seismotectonic Interpretation*), the vertical offsets are distributed on several fault branches. In any case, this would lead to an underestimation of the earthquake magnitude. In contrast, calculation of the magnitude derived from subaqueous surface ruptures can also lead to an overestimation of the earthquake magnitude. This has been reported, for example in the Aysén fjord for the M_W 6.2 earthquake in CE 2007, where coseismic subaqueous surface ruptures were larger than the underlying fault rupture in the bedrock (Wils et al., 2018).Therefore, we refrain from any detailed offset-magnitude calculations for the different fault generations and propose a minimum magnitude range of M_W 6–6.5 for the on-fault paleoseismic evidence recorded in Achensee. Given all above considerations, we propose seismotectonic activity along a NW-SE striking fault at Achensee, which produced three significant earthquakes with magnitudes M_W ~6.0–6.5 in Late Glacial to Early Holocene times. This is in accordance with semi-quantitative considerations of the off-fault paleoseismic evidence, where event horizon G contemporaneous to fault activity (generation I) by far shows the largest mass-wasting imprint in the lake. A M_W ~6.0–6.5 type earthquake at 5–10 km depth, i.e., the typical focal depth of recent seismicity at the Inn valley (Reiter et al., 2018), would produce epicentral intensities of VIII½ to X¼ (Shebalin, 1958). Such intensity values are well above the inferred threshold of ~VI, which confirms that the on-fault and off-fault evidence is consistent with each other.

Natural and Methodological Factors Influencing the Lacustrine Seismograph

MTD stratigraphy and variable sedimentation rates

The elaboration of an MTD event stratigraphy is affected by several methodological uncertainties varying from e.g. missing small MTDs due to missing coverage of the (2D) seismic grid, and difficulties in differentiating stacked MTDs to operator subjectivity in assigning MTDs to stratigraphic horizons (Moernaut et al., 2019). In our study, the very dense seismic grid allows for a quasi-complete mapping in which all MTDs larger than ~50 m in width can be identified. Many small MTDs on the slopes of the Pertisau delta may have been overlooked due to repeated delta instability and limited acoustic penetration. As earthquakes with seismic intensity > ~VI can induce sediment failure on most other slopes as well (e.g. imprint of Hall in CE 1670), this does not affect the identification of significant paleo-earthquakes, but only leads to underestimation of MTD number and total volume. Moreover, caution is needed when interpreting the cause of multiple MTDs on a seismic-stratigraphic horizon in the uppermost part of the sequence. According to the principles of lake paleoseismology, this can be interpreted as evidence for seismic shaking. Alternatively, human-induced near-coast instabilities within a short period (few decades) can produce a very similar signature on the reflection seismic data and detailed investigations of multiple sediment cores are required for a correct interpretation, as exemplified by the studies on the sedimentary archive of Lake Zurich and Wörthersee (Strasser et al., 2013; Daxer et al., 2019). In Achensee, this applies to event horizon A, which is inferred to represent a period of enhanced shoreline erosion caused by lake level changes associated to hydropower use of the lake.

The investigated Pertisau and Main basin represent two independent natural seismographs with a different temporal evolution in terms of sensitivity and completeness of off-fault paleoseismic evidence. The differences in completeness relate to the missing seismic penetration of the deeper U2 in the Main basin compared to ~40 ms visible stratigraphy in the Pertisau

basin (**Figure 3**). Moreover, U3 is condensed in the Pertisau basin compared to the Main basin indicating significantly lower sedimentation rates. Age-depth models of cores in both basins (**Figures 10A,B**) show a drastically decreased sedimentation rate in the aftermath of event horizon G, which remained low for more than 7,000 years and is associated with a change in lithostratigraphy towards less clastic, more organic-rich sediment (**Figure 9**). This abrupt change together with long-lasting lowered sedimentation rate indicate a lake or catchment-wide system change. Whether this system change was caused by a regional change in hydroclimatic pattern (Spötl et al., 2010) or local environmental effects related to the occurrence of the severe paleo-earthquake at ~8.3 ka BP remains unknown. In any case, lower sedimentation rates imply a slower charging of subaqueous slopes with fresh sediments, and therefore, the probability of earthquake-induced subaqueous mass-wasting may be lower, leading to a less sensitive lacustrine seismograph (Wilhelm et al., 2016). This may explain the absence of sedimentary evidence in the Pertisau Basin for events C, D and F, which happened during a period with the lowest sedimentation rates (~0.1 mm/year) in this basin. This highlights the key value of integrating multiple basins with different sedimentation rates and dynamics to counteract such possible under-recording of paleo-earthquakes.

Faulting of lake sediments

As alternative to a tectonic origin, subaqueous faults can also be caused by differential compaction or gravitational faults. At Achensee these alternative processes can be reasonably ruled out. Differential compaction of basin and slope sediments would cause normal faults parallel to the main axis of the basin. Although this is partly observed by the general SE-NW trend, differential compaction would not generate the observed splay of fault traces (**Figure 6A**) and would have also affected the opposite (NE) basin slope. Moreover, it cannot explain the offsets of top-U1 and the offsets in the shallow (SE) parts of the Pertisau basin (**Figure 4E**). Furthermore, differential compaction is rather a continuous process, which would not lead to the observed generation-type fault activity. Gravitational subaqueous faults caused by a deep-seated gravitational slope deformation in the SW of the Pertisau basin would generate SW-dipping thrust faults in the toe domain with top NE motions which is not observed in Achensee.

Independent of their underlying process, the preservation of subaqueous faults and our ability to map these is strongly dependent on the occurrence of marker horizons and a positive sedimentation rate–fault displacement ratio (Barnes and Pondard, 2010). In Achensee, seismic stratigraphy can be conclusively correlated across the subaqueous faults with a few limitations. These involve a laterally variable seismic facies (non-continuous to chaotic reflections) and the occurrence of prograding fan deltas in the basal part of U2. Locally, the occurrence of the DCC challenges reliable fault mapping because large-scale gravitational mass movements deformed the underlying basin sediments. Traces of the DCC-related thrusts are sub-parallel to the fault traces of interpreted tectonic origin in map view (**Figure 6A**) and one could misinterpret this by solely analysing the bottom morphology without supporting information from seismic profiles. This apparent spatial relationship is either coincidental or due to difficulties in distinguishing tectonically induced faults and thrusts related to the DCC. At least the SW thrust related to the DCC could alternatively be interpreted as a generation I tectonic fault (**Figure 4C**), but crosscutting relationships and thus genetic interpretations remain ambiguous in this area. Subaqueous fault mapping at steeper slopes is also hampered by non-conclusive stratigraphic correlation across the fault due to lowered sedimentation rates at the slopes compared to the basin and due to geometry effects on the single-channel seismic data. In the shallow SE-most Pertisau basin (**Figure 4E**), where theoretically the total offset is accommodated at a single fault, a fault growth sequence is not distinguishable due to comparably low sedimentation rates (~4 m for U3 resulting in 0.38 mm/year), potentially highly dynamic coastal sedimentary processes or due to dominating horizontal displacement. Potentially incomplete identification of reactivated faults is suggested in the fault trace map of generation II (**Figure 6C**), where the NE-most fault trace outlies the general SE-NW fault trend. A rupture on this outlying fault trace only makes sense when there are other coeval ruptures along strike (e.g., the generation III fault traces; **Figure 6D**). Potential reasons for incomplete fault identification can be that seismic penetration does not always allow for distinction or assignment of faults to their respective generation, or that faults with displacements below the vertical seismic resolution might be missed. Altogether, this evaluation suggests that fault trace identification is of good quality in the central part of the Pertisau basin, whereas the DCC in the NW part may have overprinted some of the on-fault evidence and steep or shallow terrain leads to more subjective fault identification. With regard to the quantification of fault throw (**Figures 5**, **6**), it is important to note that some of the apparent vertical offsets could be produced through a lateral slip component and oblique displacement of topographic features. This could explain the rather high values of measured fault throw when compared to the estimated potential magnitude (M_W 6–6.5) of the causative earthquakes (Stirling et al., 2002). In contrast, in a strike-slip dominant fault system, analysis of apparent vertical offsets in seismic data would probably lead to an underestimation of the earthquake magnitude.

In comparison with previous subaqueous on-fault observations in Alpine lakes with only limited stratigraphic and temporal constraints for surface rupturing events (de La Taille et al., 2015; Fabbri et al., 2017; Gasperini et al., 2020), the surface ruptures in Achensee contain i) a conclusively mappable fault growth sequence by stratigraphic marker horizons, ii) constraints for multiple rupturing events based on fault throw measurements, iii) surface rupturing events backed up by off-fault paleoseismic evidence and iv) good time constraints through sediment core data.

Seismotectonic Interpretation

The identified and mapped NW-aligned fault zone in the sedimentary infill of Achensee is interpreted as the surface expression within water-saturated sediments of coseismic bedrock deformation on the Pertisau fault. Within the

prevalent NNW-SSE present-day stress field derived from focal mechanism data (Reiter et al., 2018), the Pertisau fault acts as a transpressive, dextral strike-slip fault. Such transpressive strike-slip bedrock motion can explain the observed fault throw reversals in the lake sediments and the generally observed elevated SW fault block (**Figure 4**). A dextral rupture component along the Pertisau fault can also explain the upward splaying of individual fault branches in the lake sediments towards the NW (**Figures 12A,B**). Dextral strike-slip motion might be dominant in the SE surface ruptures, whereas almost pure normal faulting along the branches of the fault splay compensates the lateral motion. If the present-day subordinate NE-SW extensional stress field had caused surface-rupturing earthquakes, the Pertisau fault would have possibly been reactivated as a normal fault. In such a scenario, also the lake sediments would exhibit normal fault sets parallel to the basement rock. However, we consider the NE-SW extensional scenario unlikely, as it cannot explain the observed lateral component of fault motion. Independent of which stress regime caused the surface rupturing earthquakes, the maximum expectable magnitude based on the dimensions of the Pertisau fault is estimated to ~ 5.6–5.8 (Wyss, 1979), which is somewhat below the inferred magnitude threshold M_W >6.0 in this region for producing surface ruptures. Therefore, we propose that the Pertisau fault ruptured together with adjacent parts of the Sulzgraben-Eben thrust at ~8.3 ka BP and two times within Late Glacial-Early Holocene times. Since there is no subaqueous surface rupture documented in Achensee for the last 8 ka, we hypothesize that postglacial rebound might have contributed to activation of these faults, as is suggested for e.g. northern Central Europe (Brandes et al., 2015) or the Central and Western Alps (Beck et al., 1996; Kremer et al., 2017).

For the other identified earthquakes, where only off-fault evidence is present in Achensee, seismic activity of nearby major and partly blind thrust faults is likely. For event C at 1,012 a BP (849–1,164 a BP), temporal overlap with the 95% probability age range of the Münster rock avalanche (928–799 a BP; 10.5 × 106 m^3; D. Sanders, pers. comm.; **Figure 1A**) may indicate synchronicity of this severe earthquake and rockslide and thus potentially earthquake-triggering of this rockslide.

Theoretically, the off-fault sedimentary imprints in Achensee could also be caused by far-field effects of an up to 75 km apart maximum credible M_W 6.5 earthquake based on an intensity prediction equation (Fäh et al., 2011). Within this E-W oriented zone of increased seismicity along the Inn valley, there are no paleoseismic archives in the East yet, against which this hypothesis or off-fault paleoseismic evidence can be tested, but two lacustrine paleoseismic archives (Plansee, Piburgersee) exist about 75 km West from Achensee (Oswald et al., 2021). By comparing the ages of these paleoseismic events to our record, there is no significant overlap except for one event recorded in Plansee at ~8.4 ka (8.3–8.5 ka BP) which overlaps within age-range with paleo-earthquake G at ~8.3 ka (8.2–8.4 ka BP) of Achensee. However, it is unlikely that these paleoseismic evidence were caused by a single earthquake, because event G in Achensee is interpreted as a local surface-rupturing earthquake and the 8.4 ka event in Plansee represents one of the strongest seismic events documented in that archive. Therefore, we rather propose two temporally and closely spaced severe earthquakes at ~8.2–8.5 ka BP compared to a single extraordinary strong earthquake.

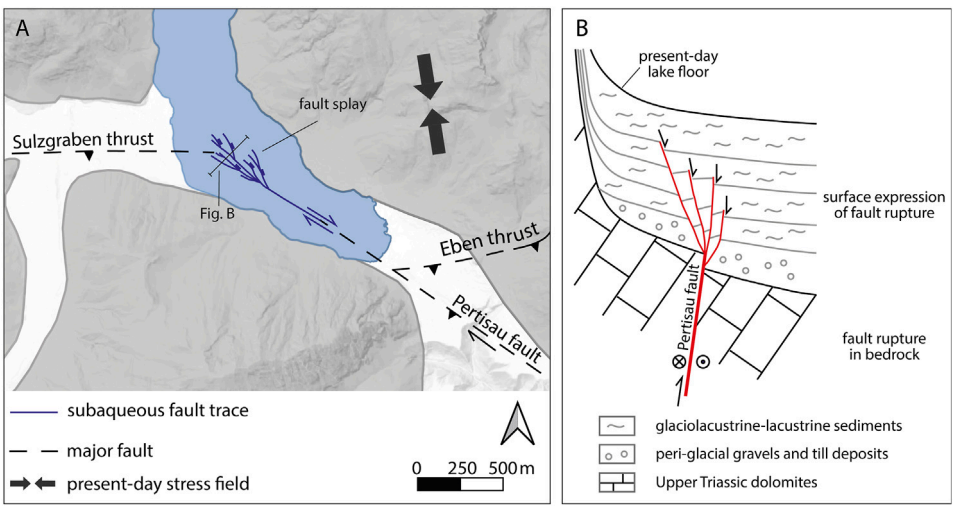

FIGURE 12 | Tectonic interpretation of the observed subaqueous fault traces in context with the present-day stress field and adjacent tectonic faults. **(A)** A dextral transpressive fault motion on the Pertisau fault together with thrusting on one or both of the Sulzgraben- and Eben thrusts is interpreted in the prevalent NNW-SSE compressional stress field. In the overlying lake sediments, this causes a general uplift of the SW block, dominant dextral faulting in the SE part and a fault splay with dominant normal faulting. **(B)** Sketched, unscaled cross section of the fault splay highlighting the difference of the fault rupture in the bedrock compared to the surface deformation within the water-saturated soft sediments. Note the general uplift of the SW fault block in the bedrock and its corresponding surface expression as normal faulting within the lake sediments near the NW end of subaqueous faults. For location of cross section see A).

CONCLUSION

We document both on-fault paleoseismic evidence as subaqueous surface ruptures and off-fault paleoseismic evidence as multiple, coeval MTDs and megaturbidites in the inner-alpine lake Achensee located in the slowly but actively deforming European Eastern Alps. This rare observation of combined on-fault and off-fault evidence in the same geological archive allows comparison of commonly applied semi-quantitative considerations to paleo-earthquakes derived from surface ruptures and mass-wasting in lakes. Furthermore, we discuss potential natural and methodological factors influencing the "natural seismograph" of subaqueous realms recording remote earthquakes and the preservation of subaqueous surface ruptures and put our paleoseismic results within the regional seismotectonic framework. The following general (1–4) and site-specific (5–6) conclusions can be drawn:

1) Glacigenic, mountain lakes such as Achensee are often located above major faults and therefore potentially form high-resolution on-fault paleoseismic archives, characterized by an excellent preservation of surface ruptures due to continuous lacustrine sedimentation. Such subaqueous records are especially valuable in low-strain intraplate regions where onshore identification of on-fault evidence is scarce or absent.
2) Subaqueous surface ruptures can exhibit different expression types in reflection seismic data such as blurred zones, intersecting hyperbolic reflections or discrete faults. The identification of a potential fault growth sequence and measurements of individual and total fault throw along a fault requires good stratigraphic control, which strongly depends on the applied seismic source and seismic facies of overlying and lateral stratigraphy. Moreover, the sedimentation rate–fault displacement ratio must be positive to preserve fault growth sequences.
3) For the application of multiple, coeval MTDs as off-fault paleoseismic evidence, sediment parameters such as a high number and total volume of MTDs and the presence of a megaturbidite may be indicative for stronger shaking above the lake-specific intensity threshold. At Achensee, this is supported by the comparison of semi-quantitative considerations of combined on-fault and off-fault paleoseismic evidence in a single stratigraphic framework.
4) A multi-basin approach can verify the quality of the individual basins as natural seismographs and can overcome potential limitations of individual basins caused by e.g. variable sedimentation rates related to external environmental effects.
5) We present first-ever on-fault Holocene paleoseismic evidence of the region (Tyrol) by pinpointing seismotectonic activity of the Sulzgraben-Eben thrust at ~8.3 ka BP and two times in the Late Glacial. For these events we propose a minimum magnitude range of M_W ~6–6.5.
6) The CE 1670 earthquake and seven prehistoric earthquakes over the last 11,000 years are recorded at Achensee by multiple, coeval mass wasting providing the first continuous Holocene paleoseismic record of eastern Tyrol.

DATA AVAILABILITY STATEMENT

The raw data supporting the conclusions of this article will be made available by the authors, without undue reservation.

AUTHOR CONTRIBUTIONS

MS, JM and PO designed the study. PO, JM and MS acquired the pinger seismics and retrieved the sediment cores. SF acquired and processed the bathymetry. MD made the Centipede sparker source available within a research collaboration. IH measured ^{14}C samples within a research collaboration. HO contributed to the integration of lake data within the seismotectonic setting. ST carried out seismic stratigraphic mapping within his MSc thesis project. PO analyzed and interpreted seismic and core data. PO created figures and PO, JM and MS wrote the manuscript with input of all co-authors.

FUNDING

This research is supported by the Tyrolean Science Fund (project UNI-16588/5-2019), the Austrian Science Fund (FWF): P30285-N34, European Regional Development Fund Interreg 312 V-A (project ITAT-301 6), Austrian Academy of Sciences ÖAW (ESS-IGCP-project S4LIDE-Austria) and Nachwuchsförderung 2016, University of Innsbruck.

ACKNOWLEDGMENTS

We thank Anton Kandler for all his onsite help, technical support and boat loan during fieldwork at Achensee. We are grateful to the countless helpers during the coring and geophysics surveys. In particular, we thank Michael Hilbe for joining the acquisition of the multibeam bathymetry survey and Flavio Anselmetti for facilitating it. Koen De Rycker is thanked for the acquisition of the sparker survey. We further thank Hans Walser for providing useful historical insights on the human influence on Achensee. We thank Markus Erhardt, Gerald Degenhart and Wolfgang Recheis for the medical CT measurements at the Medical University of Innsbruck. We also thank the reviewers KK and GR for their constructive comments. Natalie Dubois is thanked for short-lived radionuclide dating. Land Tirol - data.tirol.gv.at is thanked for providing the DEM data. IHS Markit is acknowledged for their educational grant program providing the Kingdom seismic interpretation software.

SUPPLEMENTARY MATERIAL

The Supplementary Material for this article can be found online at: https://www.frontiersin.org/articles/10.3389/feart.2021.670952/full#supplementary-material

REFERENCES

Ampferer, O. (1928). Die Reliefüberschiebung des Karwendelgebirges. *Jahrb. der Geol. Bundesanstalt* 78, 241–256.

Ampferer, O., and Ohnesorge, T. (1924). *Erläuterungen zur Geologischen Spezial-Karte der Republik Österreich Blatt Innsbruck-Achensee (5047)*. Wien: Geol. Bundesanstalt.

Ampferer, O., and Pinter, K. (1927). Über geologische und technische Erfahrungen beim Bau des Achenseewerkes in Tirol. *Jahrb. der Geol. Bundesanstalt* 77, 279–332.

Barnes, P. M., and Audru, J.-C. (1999). Recognition of Active Strike-Slip Faulting from High-Resolution marine Seismic Reflection Profiles: Eastern Marlborough Fault System, New Zealand, *Bull. Geol. Soc. Am.* 111, 538–559. doi:10.1130/0016-7606(1999)111<053810.1130/0016-7606(1999)111<0538:roassf>2.3.co;2

Barnes, P. M., and Pondard, N. (2010). Derivation of Direct On-Fault Submarine Paleoearthquake Records from High-Resolution Seismic Reflection Profiles: Wairau Fault, New Zealand. *Geochem. Geophys. Geosyst.* 11, a–n. doi:10.1029/2010GC003254

Beck, C., Manalt, F., Chapron, E., Rensbergen, P. V., and Batist, M. D. (1996). Enhanced Seismicity in the Early post-glacial Period: Evidence from the post-würm Sediments of lake Annecy, Northwestern Alps. *J. Geodynamics*. 22, 155–171. doi:10.1016/0264-3707(96)00001-4

Beck, C., Reyss, J.-L., Leclerc, F., Moreno, E., Feuillet, N., Barrier, L., et al. (2012). Identification of Deep Subaqueous Co-seismic Scarps through Specific Coeval Sedimentation in Lesser Antilles: Implication for Seismic hazard. *Nat. Hazards Earth Syst. Sci.* 12, 1755–1767. doi:10.5194/nhess-12-1755-2012

Bellwald, B., Hjelstuen, B. O., Sejrup, H. P., and Haflidason, H. (2016). "Postglacial Mass Failures in the Inner Hardangerfjorden System, Western Norway," in *"Postglacial Mass Failures in the Inner Hardangerfjorden System, Western Norway," in* Submarine Mass Movements And Their Consequences. G. Lamarche, J. Mountjoy, S. Bull, T. Hubble, S. Krastel, E. Lane, et al. (Springer Netherlands), 73–82. doi:10.1007/978-3-319-20979-1_7

Blaauw, M., and Christen, J. A. (2011). Flexible Paleoclimate Age-Depth Models Using an Autoregressive Gamma Process. *Bayesian Anal.* 6, 457–474. doi:10.1214/11-BA61810.1214/ba/1339616472

Bouroullec, R., Cartwright, J. A., Johnson, H. D., Lansigu, C., Quémener, J.-M., and Savanier, D. (2004). Syndepositional Faulting in the Grès d'Annot Formation, SE France: High-Resolution Kinematic Analysis and Stratigraphic Response to Growth Faulting. *Geol. Soc. Lond. Spec. Publications* 221, 241–265. doi:10.1144/GSL.SP.2004.221.01.13

Bousquet, R., Schmid, S. M., Zeilinger, G., Oberhänsli, R., Rosenberg, C., and Molli, G. (2012). Tectonic framework of the Alps, (scale 1:1.000.000). *Commission for the Geological Map of the World*. Available at: https://www.researchgate.net/publication/341579276_Tectonic_framework_of_the_Alps.

Brandes, C., Steffen, H., Steffen, R., and Wu, P. (2015). Intraplate Seismicity in Northern Central Europe Is Induced by the Last Glaciation. *Geology*. 43, 611–614. doi:10.1130/G36710.1

Brandner, R. (1980). *Geologische Übersichtskarte von Tirol, (1:300.000)*. Innsbruck: Universitätsverlag Wagner

Brengman, C. M. J., Barnhart, W. D., Mankin, E. H., and Miller, C. N. (2019). Earthquake-Scaling Relationships from Geodetically Derived Slip Distributions. *Bull. Seismol. Soc. Am.* 109, 1701–1715. doi:10.1785/0120190048

Bull, J. M., Barnes, P. M., Lamarche, G., Sanderson, D. J., Cowie, P. A., Taylor, S. K., et al. (2006). High-resolution Record of Displacement Accumulation on an Active normal Fault: Implications for Models of Slip Accumulation during Repeated Earthquakes. *J. Struct. Geology* 28, 1146–1166. doi:10.1016/j.jsg.2006.03.006

Burschil, T., Tanner, D. C., Reitner, J. M., Buness, H., and Gabriel, G. (2019). Unravelling the Shape and Stratigraphy of a Glacially-Overdeepened valley with Reflection Seismic: the Lienz Basin (Austria). *Swiss J. Geosci.* 112, 341–355. doi:10.1007/s00015-019-00339-0

Cartwright, J., Bouroullec, R., James, D., and Johnson, H. (1998). Polycyclic Motion History of Some Gulf Coast Growth Faults from High-Resolution Displacement Analysis, *Geol.* 26:819–822. doi:10.1130/0091-7613(1998)026<0819:PMHOSG>2.310.1130/0091-7613(1998)026<0819:pmhosg>2.3.co;2

Costantini, D., and Ortner, H. (2013). Klüfte und Deformationsstrukturen in jungpleistozänen Beckensedimenten des Rißtales, Bayern. *Geo.Alp*. 10, 5–26.

Daxer, C., Moernaut, J., Taylor, T., Haas, J. N., and Strasser, M. (2018). Late Glacial and Holocene Sedimentary Infill of Lake Mondsee (Eastern Alps, Austria) and Historical rockfall Activity Revealed by Reflection Seismics and Sediment Core Analysis. *Austrian J. Earth Sci.* 111, 111–134. doi:10.17738/ajes.2018.0008

Daxer, C., Sammartini, M., Molenaar, A., Piechl, T., Strasser, M., and Moernaut, J. (2019). Morphology and Spatio-Temporal Distribution of Lacustrine Mass-Transport Deposits in Wörthersee, Eastern Alps, Austria, *Geol. Soc. London, Spec. Publ.*, 500, 235–254. doi:10.1144/sp500-2019-179

de La Taille, C., Jouanne, F., Crouzet, C., Beck, C., Jomard, H., de Rycker, K., et al. (2015). Impact of Active Faulting on the post LGM Infill of Le Bourget Lake (Western Alps, France). *Tectonophysics* 664, 31–49. doi:10.1016/j.tecto.2015.08.024

Eisbacher, G. H., and Brandner, R. (1996). Superposed Fold-Thrust Structures and High-Angle Faults, Northwestern Calcareous Alps, Austria. *Eclogae Geol. Helv.* 89, 553–571.

Fabbri, S. C., Buechi, M. W., Horstmeyer, H., Hilbe, M., Hübscher, C., Schmelzbach, C., et al. (2018). A Subaquatic Moraine Complex in Overdeepened Lake Thun (Switzerland) Unravelling the Deglaciation History of the Aare Glacier. *Quat. Sci. Rev.* 187, 62–79. doi:10.1016/j.quascirev.2018.03.010

Fabbri, S. C., Herwegh, M., Horstmeyer, H., Hilbe, M., Hübscher, C., Merz, K., et al. (2017). Combining Amphibious Geomorphology with Subsurface Geophysical and Geological Data: A Neotectonic Study at the Front of the Alps (Bernese Alps, Switzerland). *Quat. Int.* 451, 101–113. doi:10.1016/j.quaint.2017.01.033

Fäh, D., Giardini, D., Kästli, P., Deichmann, N., Gisler, M., Schwarz-Zanetti, G., et al. (2011). *ECOS-09 Earthquake Catalogue of Switzerland ReleaseReport and DataPublic Catalogue, 17.04*. Zurich: Swiss Seismol. Serv. ETH Zurich.

Galadini, F., and Galli, P. (1999). Palaeoseismology Related to the Displaced Roman Archaeological Remains at Egna (Adige Valley, Northern Italy). *Tectonophysics* 308, 171–191. doi:10.1016/S0040-1951(99)00080-3

Gasperini, L., Marzocchi, A., Mazza, S., Miele, R., Meli, M., Najjar, H., et al. (2020). Morphotectonics and Late Quaternary Seismic Stratigraphy of Lake Garda (Northern Italy). *Geomorphology*. 371, 107427. doi:10.1016/j.geomorph.2020.107427

Gastineau, R., Sigoyer, J., Sabatier, P., Fabbri, S. C., Anselmetti, F. S., Develle, A. L., et al. (2021). Active Subaquatic Fault Segments in Lake Iznik along the Middle Strand of the North Anatolian Fault, NW Turkey. *Tectonics* 40. doi:10.1029/2020tc006404

Geologische Bundesanstalt (2021a). GEOFAST, Compiled Geological Maps of Austria (WMS Service). Vienna. Available at: https://gisgba.geologie.ac.at/arcgis/services/projekte_geofast/AT_GBA_GEOFAST_MS/MapServer/WMSServer? (Accessed January 15, 2021).

Geologische Bundesanstalt (2021b). *Geological Maps of Austria 1:50.000 (WMS Service)*. Vienna. Available at: https://gisgba.geologie.ac.at/arcgis/services/image/AT_GBA_GK50_MapS/MapServer/WMSServer? (Accessed January 15, 2021).

Gilli, A., Anselmetti, F. S., Glur, L., and Wirth, S. B. (2013). "Lake Sediments as Archives of Recurrence Rates and Intensities of Past Flood Events," in *Dating Torrential Processes on Fans and Cones Advances in Global Change Research*. Editors M. Schneuwly-Bollschweiler, M. Stoffel, and F. Rudolf-Miklau (Dordrecht: Springer Netherlands), 225–242. doi:10.1007/978-94-007-4336-6

Gruber, A., and Brandner, R. (2012). *Geologische Karte der Republik Österreich 1: 50.000, Blatt 88 Achenkirch*. Vienna: Geologischen Bundesanstalt

Hilbe, M., Anselmetti, F. S., and Eyles, N. (2014). Signatures of Slope Failures and River-delta Collapses in a Perialpine lake (Lake Lucerne, Switzerland). *Sedimentology*. 61, 1883–1907. doi:10.1111/sed.12120

Howarth, J. D., Fitzsimons, S. J., Norris, R. J., Langridge, R., and Vandergoes, M. J. (2016). A 2000 Yr Rupture History for the Alpine Fault Derived from Lake Ellery, South Island, New Zealand. *Geol. Soc. America Bull.* 128, 627–643. doi:10.1130/B31300.1

Irmler, R., Daut, G., and Mäusbacher, R. (2006). A debris flow calendar derived from sediments of lake Lago di Braies (N. Italy). *Geomorphology*. 77, 69–78. doi:10.1016/j.geomorph.2006.01.013

Kelts, K., Briegel, U., Ghilardi, K., and Hsu, K. (1986). The Limnogeology-ETH Coring System. *Schweiz. Z. Hydrol.* 48, 104–115. doi:10.1007/BF02544119

Kilian, S., and Ortner, H. (2019). Structural Evidence of In-Sequence and Out-Of-Sequence Thrusting in the Karwendel Mountains and the Tectonic Subdivision

of the Western Northern Calcareous Alps. *Austrian J. Earth Sci.* 112, 62–83. doi:10.17738/ajes.2019.0005

Krauter, V. E. (1967). *Zur Frage der Reliefüberschiebung am Staner-Joch (östliches Karwendel , Tirol)*. Mitteilungen der Geol. Gesellschaft Wien, 23–64.

Kremer, K., Gassner-Stamm, G., Grolimund, R., Wirth, S. B., Strasser, M., and Fäh, D. (2020). A Database of Potential Paleoseismic Evidence in Switzerland. *J. Seismol.* 24, 247–262. doi:10.1007/s10950-020-09908-5

Kremer, K., Wirth, S. B., Reusch, A., Fäh, D., Bellwald, B., Anselmetti, F. S., et al. (2017). Lake-sediment Based Paleoseismology: Limitations and Perspectives from the Swiss Alps. *Quat. Sci. Rev.* 168, 1–18. doi:10.1016/j.quascirev.2017.04.026

Lenhardt, W. A., Freudenthaler, C., Lippitsch, R., and Fiegweil, E. (2007). Focal-depth Distributions in the Austrian Eastern Alps Based on Macroseismic Data. *Austrian J. Earth Sci.* 100, 66–79.

Métois, M., D'Agostino, N., Avallone, A., Chamot-Rooke, N., Rabaute, A., Duni, L., et al. (2015). Insights on continental Collisional Processes from GPS Data: Dynamics of the peri-Adriatic Belts. *J. Geophys. Res. Solid Earth*. 120, 8701–8719. doi:10.1002/2015JB012023

Mey, J., Scherler, D., Wickert, A. D., Egholm, D. L., Tesauro, M., Schildgen, T. F., et al. (2016). Glacial Isostatic Uplift of the European Alps. *Nat. Commun.* 7, 1–10. doi:10.1038/ncomms13382

Mitchum, R. M., Vail, P. R., and Sangree, J. B. (1977). "Seismic Stratigraphy and Global Changes of Sea Level, Part 6Stratigraphic Interpretation of Seismic Reflection Patterns in Depositional Sequences1," in *Seismic Stratigraphy — Applications To Hydrocarbon Exploration*. Editor C. E. Payton (American Association of Petroleum Geologists Memoir), 117–133. doi:10.1306/M26490C8

Moernaut, J., Daele, M. V., Heirman, K., Fontijn, K., Strasser, M., Pino, M., et al. (2014). Lacustrine Turbidites as a Tool for Quantitative Earthquake Reconstruction: New Evidence for a Variable Rupture Mode in South central Chile. *J. Geophys. Res. Solid Earth* 119, 1607–1633. doi:10.1002/2013JB010738

Moernaut, J. (2020). Time-dependent Recurrence of strong Earthquake Shaking Near Plate Boundaries: A lake Sediment Perspective. *Earth-Science Rev.* 210, 103344. doi:10.1016/j.earscirev.2020.103344

Moernaut, J., van Daele, M., Heirman, K., Wiemer, G., Molenaar, A., Vandorpe, T., et al. (2019). The Subaqueous Landslide Cycle in South-central Chilean Lakes: The Role of Tephra, Slope Gradient and Repeated Seismic Shaking. *Sediment. Geology.* 381, 84–105. doi:10.1016/j.sedgeo.2019.01.002

Monecke, K., Anselmetti, F. S., Becker, A., Sturm, M., and Giardini, D. (2004). The Record of Historic Earthquakes in lake Sediments of Central Switzerland. *Tectonophysics* 394, 21–40. doi:10.1016/j.tecto.2004.07.053

Moser, M. (2008). *Geofast - Zusammenstellung ausgewählter Archivunterlagen der Geologischen Bundesanstalt 1:50.000 - 119 Schwaz*. Vienna: Geologische Bundesanstalt.

Ndiaye, M., Clerc, N., Gorin, G., Girardclos, S., and Fiore, J. (2014). Lake Neuchâtel (Switzerland) Seismic Stratigraphic Record Points to the Simultaneous Würmian Deglaciation of the Rhône Glacier and Jura Ice Cap. *Quat. Sci. Rev.* 85, 1–19. doi:10.1016/j.quascirev.2013.11.017

Ortner, H., Aichholzer, S., Zerlauth, M., Pilser, R., and Fügenschuh, B. (2015). Geometry, Amount, and Sequence of Thrusting in the Subalpine Molasse of Western Austria and Southern Germany, European Alps. *Tectonics* 34, 1–30. doi:10.1002/2014TC003550

Ortner, H., Reiter, F., and Brandner, R. (2006). Kinematics of the Inntal Shear Zone-Sub-Tauern Ramp Fault System and the Interpretation of the TRANSALP Seismic Section, Eastern Alps, Austria. *Tectonophysics* 414, 241–258. doi:10.1016/j.tecto.2005.10.017

Oswald, P., Strasser, M., Hammerl, C., and Moernaut, J. (2021). Seismic Control of Large Prehistoric Rockslides in the Eastern Alps. *Nat. Commun.* 12. doi:10.1038/s41467-021-21327-9

Pinson, L. J. W., Vardy, M. E., Dix, J. K., Henstock, T. J., Bull, J. M., and Maclachlan, S. E. (2013). Deglacial History of Glacial lake windermere, UK: Implications for the central British and Irish Ice Sheet. *J. Quat. Sci.* 28, 83–94. doi:10.1002/jqs.2595

Plan, L., Grasemann, B., Spötl, C., Decker, K., Boch, R., and Kramers, J. (2010). Neotectonic Extrusion of the Eastern Alps: Constraints from U/Th Dating of Tectonically Damaged Speleothems. *Geology* 38, 483–486. doi:10.1130/g30854.1

Poscher, G. (1994). Fazies und Genese der pleistozänen Terrassensedimente im Tiroler Inntal und seinen Seitentälern - Teil 1: Der Achenseedamm. *Jahrb. der Geol. Bundesanstalt* 137, 171–186.

Praet, N. (2020). *Towards the Construction of a Lacustrine Paleoseismic Record in South-central Alaska : a Trembling Tale of Landslides and Turbidites*. Ghent: Universiteit Gent. . Faculteit Wetenschappen Available at:http://hdl.handle.net/1854/LU-8681726 (Accessed February 14, 2021).

Preusser, F., Reitner, J. M., and Schlüchter, C. (2010). Distribution, Geometry, Age and Origin of Overdeepened Valleys and Basins in the Alps and Their Foreland. *Swiss J. Geosci.* 103, 407–426. doi:10.1007/s00015-010-0044-y

Rapuc, W., Sabatier, P., Andrič, M., Crouzet, C., Arnaud, F., Chapron, E., et al. (2018). 6600 Years of Earthquake Record in the Julian Alps (Lake Bohinj, Slovenia). *Sedimentology*. 65, 1777–1799. doi:10.1111/sed.12446

Ratschbacher, L., Merle, O., Davy, P., and Cobbold, P. (1991). Lateral Extrusion in the Eastern Alps, Part 1: Boundary Conditions and Experiments Scaled for Gravity. *Tectonics* 10, 245–256. doi:10.1029/90TC02622

Reimer, P. J., Austin, W. E. N., Bard, E., Bayliss, A., Blackwell, P. G., Bronk Ramsey, C., et al. (2020). The IntCal20 Northern Hemisphere Radiocarbon Age Calibration Curve (0-55 Cal kBP). *Radiocarbon*. 62, 725–757. doi:10.1017/RDC.2020.41

Reiter, F., Freudenthaler, C., Hausmann, H., Ortner, H., Lenhardt, W., and Brandner, R. (2018). Active Seismotectonic Deformation in Front of the Dolomites Indenter, Eastern Alps. *Tectonics* 37, 4625–4654. doi:10.1029/2017TC004867

Ritz, J.-F., Baize, S., Ferry, M., Larroque, C., Audin, L., Delouis, B., et al. (2020). Surface Rupture and Shallow Fault Reactivation during the 2019 Mw 4.9 Le Teil Earthquake, France. *Commun. Earth Environ.* 1, 1–11. doi:10.1038/s43247-020-0012-z

Robl, J., and Stüwe, K. (2005). Continental Collision with Finite Indenter Strength: 2. European Eastern Alps. *Tectonics* 24, a–n. doi:10.1029/2004TC001741

Rosenberg, C. L., Brun, J.-P., and Gapais, D. (2004). Indentation Model of the Eastern Alps and the Origin of the Tauern Window. *Geol.* 32, 997–1000. doi:10.1130/G20793.1

Sammartini, M., Moernaut, J., Anselmetti, F. S., Hilbe, M., Lindhorst, K., Praet, N., et al. (2019). ""An Atlas of Mass-Transport Deposits in Lakes," in *In Submarine Landslides: Subaqueous Mass Transport Deposits From Outcrops To Seismic Profiles*. Editors K. Ogeta, A. Festa, and G. A. Pini (Washington: American Geophysical Union), 201–226. Available at: https://onlinelibrary.wiley.com/doi/abs/10.1002/9781119500513.ch13.

Sammartini, M., Moernaut, J., Kopf, A., Stegmann, S., Fabbri, S. C., Anselmetti, F. S., et al. (2021). Propagation of Frontally Confined Subaqueous Landslides: Insights from Combining Geophysical, Sedimentological, and Geotechnical Analysis. *Sediment. Geology.* 416, 105877. doi:10.1016/j.sedgeo.2021.105877

Schnellmann, M., Anselmetti, F. S., Giardini, D., and Mckenzie, J. A. (2006). 15,000 Years of Mass-Movement History in Lake Lucerne: Implications for Seismic and Tsunami Hazards. *Eclogae Geol. Helv.* 99, 409–428. doi:10.1007/s00015-006-1196-7

Schnellmann, M., Anselmetti, F. S., Giardini, D., Mckenzie, J. A., and Ward, S. N. (2002). Prehistoric Earthquake History Revealed by Lacustrine Slump Deposits, *Geol.* 30, 1131–1134. doi:10.1130/0091-7613(2002)030<1131:PEHRBL>2.010.1130/0091-7613(2002)030<1131:pehrbl>2.0.co;2

Shebalin, N. (1958). Correlation between Earthquake Magnitude and Intensity. *Stud. Geophys. Geod.* 2, 86–87.

Sossau, C. (1995). Achensee: Limnologische Untersuchung nach der Abwassersanierung seines Einzugsgebiet. *Stud. Im Auftrag Des Amts der Tiroler Landesregierung*, 98.

Spötl, C., Nicolussi, K., Patzelt, G., and Boch, R. (2010). Humid Climate during Deposition of Sapropel 1 in the Mediterranean Sea: Assessing the Influence on the Alps. *Glob. Planet. Change*. 71, 242–248. doi:10.1016/j.gloplacha.2009.10.003

Stirling, M., Rhoades, D., and Berryman, K. (2002). Comparison of Earthquake Scaling Relations Derived from Data of the Instrumental and Preinstrumental Era. *Bull. Seismological Soc. America* 92, 812–830. doi:10.1785/0120000221

Strasser, M., Anselmetti, F. S., Fäh, D., Giardini, D., and Schnellmann, M. (2006). Magnitudes and Source Areas of Large Prehistoric Northern Alpine Earthquakes Revealed by Slope Failures in Lakes. *Geol.* 34, 1005. doi:10.1130/G22784A.1

Strasser, M., Berberich, T., Fabbri, S., Hilbe, M., Huang, J.-J. S., Lauterbach, S., et al. (2020). Geomorphology and Event-Stratigraphy of Recent Mass-Movement Processes in Lake Hallstatt (UNESCO World Heritage Cultural Landscape, Austria). *Geol. Soc. Lond. Spec. Publications*. 500, 405–426. doi:10.1144/sp500-2019-178

Strasser, M., Monecke, K., Schnellmann, M., and Anselmetti, F. S. (2013). Lake Sediments as Natural Seismographs: A Compiled Record of Late Quaternary Earthquakes in Central Switzerland and its Implication for Alpine Deformation. *Sedimentology* 60, 319–341. doi:10.1111/sed.12003

Stucchi, M., Rovida, A., Gomez Capera, A. A., Alexandre, P., Camelbeeck, T., Demircioglu, M. B., et al. (2013). The SHARE European Earthquake Catalogue (SHEEC) 1000-1899. *J. Seismol.* 17, 523–544. doi:10.1007/s10950-012-9335-2

Ustaszewski, M., and Pfiffner, O. a. (2008). Neotectonic Faulting, Uplift and Seismicity in the central and Western Swiss Alps. *Geol. Soc. Lond. Spec. Publications*. 298, 231–249. doi:10.1144/SP298.12

Van Daele, M., Haeussler, P. J., Witter, R. C., Praet, N., and De Batist, M. (2019). The Sedimentary Record of the 2018 Anchorage Earthquake in Eklutna Lake, Alaska: Calibrating the Lacustrine Seismograph. *Seismol. Res. Lett.* 91, 126–141. doi:10.1785/0220190204

Van Daele, M., Meyer, I., Moernaut, J., De Decker, S., Verschuren, D., and De Batist, M. (2017). A Revised Classification and Terminology for Stacked and Amalgamated Turbidites in Environments Dominated by (Hemi)pelagic Sedimentation. *Sediment. Geology.* 357, 72–82. doi:10.1016/j.sedgeo.2017.06.007

Van Daele, M., Moernaut, J., Doom, L., Boes, E., Fontijn, K., Heirman, K., et al. (2015). A Comparison of the Sedimentary Records of the 1960 and 2010 Great Chilean Earthquakes in 17 Lakes: Implications for Quantitative Lacustrine Palaeoseismology. *Sedimentology*. 62, 1466–1496. doi:10.1111/sed.12193

Van Rensbergen, P., De Batist, M., Beck, C., and Manalt, F. (1998). High-resolution Seismic Stratigraphy of Late Quaternary Fill of Lake Annecy (Northwestern Alps): Evolution from Glacial to Interglacial Sedimentary Processes. *Sediment. Geology.* 117, 71–96. doi:10.1016/S0037-0738(97)00123-1

Wilhelm, B., Arnaud, F., Sabatier, P., Magand, O., Chapron, E., Courp, T., et al. (2013). Palaeoflood Activity and Climate Change over the Last 1400 Years Recorded by lake Sediments in the north-west European Alps. *J. Quat. Sci.* 28, 189–199. doi:10.1002/jqs.2609

Wilhelm, B., Nomade, J., Crouzet, C., Litty, C., Sabatier, P., Belle, S., et al. (2016). Quantified Sensitivity of Small lake Sediments to Record Historic Earthquakes: Implications for Paleoseismology. *J. Geophys. Res. Earth Surf.* 121, 2–16. doi:10.1002/2015JF003644

Wils, K., van Daele, M., Lastras, G., Kissel, C., Lamy, F., and Siani, G. (2018). Holocene Event Record of Aysén Fjord (Chilean Patagonia): An Interplay of Volcanic Eruptions and Crustal and Megathrust Earthquakes. *J. Geophys. Res. Solid Earth*. 123, 324–343. doi:10.1002/2017JB014573

Wölfler, A., Kurz, W., Fritz, H., and Stüwe, K. (2011). Lateral Extrusion in the Eastern Alps Revisited: Refining the Model by Thermochronological, Sedimentary, and Seismic Data. *Tectonics* 30, a–n. doi:10.1029/2010TC002782

Wyss, M. (1979). Estimating Maximum Expectable Magnitude of Earthquakes from Fault Dimensions, *Geol.* 7, 336–340. doi:10.1130/0091-7613(1979)7<33610.1130/0091-7613(1979)7<336:ememoe>2.0.co;2

Zalan, P. V. (1987). Identification of Strike-slip Faults in Seismic Sections. *SEG Annu. Meet.*, 116–118. doi:10.1190/1.1892142

Conflict of Interest: The authors declare that the research was conducted in the absence of any commercial or financial relationships that could be construed as a potential conflict of interest.